

# Bayesian inference for aggregated Hawkes processes

Lingxiao Zhou and Georgia Papadogeorgou \*

Department of Statistics, University of Florida

## Abstract

The Hawkes process, a self-exciting point process, has a wide range of applications in modeling earthquakes, social networks and stock markets. The established estimation process requires that researchers have access to the exact time stamps and marks. However, available data are often rounded or aggregated. We develop a Bayesian estimation procedure for the parameters of a Hawkes process based on aggregated data. Our approach is developed for temporal, spatio-temporal, and mutually exciting Hawkes processes where data are available over discrete time periods and regions. The method is demonstrated on simulated temporal and spatio-temporal data in the presence of one or more interacting processes, and under varying coarseness of data aggregation. Finally, we analyze spatio-temporal point pattern data of insurgent attacks in Iraq from October to December 2006, and we find coherent results across different time and space aggregations.

## 1 Introduction

Point pattern data are ubiquitous across a number of applied fields, and understanding the underlying dynamics generating these patterns is the goal of point pattern modeling. A type of dynamic that is often of explicit interest is that of self-excitement, referring to the case where the occurrence of an event triggers subsequent events. A common model for studying excitement in point pattern data is the Hawkes process (Hawkes, 1971). With initial application in seismology (Ogata, 1998), Hawkes processes have been used to study terrorist attacks (Porter and White, 2012; Lewis *et al.*, 2012), financial markets (Lapham, 2014) and in epidemiology (Chiang *et al.*, 2022), among other areas. Their wide use and applicability has led to extensive

---

\*This material is based upon work supported by the National Science Foundation under Grant No. 2124124.

research on precise and computationally efficient estimation of model parameters, within the frequentist (Veen and Schoenberg, 2008) and the Bayesian (Rasmussen, 2013) paradigm. In addition to the exact time of an event’s occurrence, researchers often have access to specific characteristics of the event, which are referred to as *marks*. In this manuscript, we focus on the special case of spatio-temporal point processes corresponding to the scenario where an event’s mark is its location. Incorporating an event’s spatial coordinates in the point process modeling can provide additional insights in the process’ self-excitement dynamics. In addition to studying *self*-excitement, the Hawkes process can incorporate mutual excitement among multiple point processes of different types. Mutually-exciting Hawkes processes provide a framework to study interaction dynamics where the occurrence of an event of one type can lead to subsequent events of the same or the other type.

Standard estimation techniques for the Hawkes process require that the exact time and location of events is known. However, real data are often only available at aggregated levels across time, space, or other marks. For example, the time of occurrence of an event might be coarsened at the day level rather than knowing the exact time stamp, some published earthquake data are aggregated over towns, and survey respondents often choose from several categories instead of reporting exact values. Since data of this form are available within bins of time, space, and marks, they could also be referred to as *binned* or *discretized*, though we maintain the term *aggregated* for the remainder of this manuscript. When data are aggregated, standard estimation and inference techniques for the underlying continuous time and space Hawkes point process are not applicable. In these cases, it is common practice to model the discretized point pattern dynamics using, for example, autoregressive models in time or space (Aldor-Noiman *et al.*, 2016; Darolles *et al.*, 2019). However, such models ignore the possible dependencies among events within the discrete bins, and they do not represent process dynamics at the scale at which they naturally occur. Even though there exists some work on inferring the underlying Hawkes process model parameters from discrete-time models based on temporal, aggregated point pattern data (Kirchner, 2016, 2017), the equivalence is only established for autoregressive models with infinite lags (which are impossible to fit), and it is not clear whether the results are sensitive to the scale of data aggregation or how the method can be extended to incorporate space, other marks, or multiple processes. Shlomovich *et al.* (2022) proposed a Monte Carlo Expectation-Maximization

(MC-EM) algorithm to estimate the parameters of a Hawkes process based on aggregated temporal data, and Shlomovich *et al.* (2021) extended it to multivariate Hawkes processes. Their approach, which is only developed for temporal point patterns, is based on an expectation-maximization algorithm which cannot be used directly for performing inference over model parameters.

In this manuscript, we propose an estimation technique for modeling point pattern data within the realm of Hawkes processes when the available data are aggregated across time, space, or both. We review the Hawkes process in Section 2. We discuss the challenge of aggregated data along with our approach in Section 3. Our approach, which is positioned within the Bayesian paradigm, is based on considering the real (continuous) time of event occurrence as latent variables. Then, we propose a Markov Chain Monte Carlo (MCMC) scheme for learning the parameters of the Hawkes process which involves straightforward imputation of these latent variables. Our approach improves on the existing methodology in a number of ways. First, it allows for aggregated point pattern data with spatial information, which can itself be available at coarse spatial regions. Second, it allows for modeling multiple, mutually-exciting Hawkes processes, each of which can be aggregated across time, space, or both, with the same or different granularity. Lastly, by placing our approach within the Bayesian framework, our estimation strategy leads to straightforward inference procedures that propagate all sources of uncertainty. We evaluate the performance of the proposed approach in terms of estimation and inference over simulated data sets (Section 4), and using real data on insurgent violence in Iraq (Section 5), under different coarseness of aggregation in time and space. We conclude with a discussion and possible extensions in Section 6.

## 2 The Hawkes process

In this section, we review the Hawkes process. We start by an introduction to the spatio-temporal Hawkes process in Section 2.1 and then extend it to the multivariate Hawkes process in Section 2.2.

### 2.1 The spatio-temporal Hawkes process

A temporal point process is a stochastic process that gives rise to events over time. In marked point processes, the occurrence of an event is also tagged with additional information on the event, referred to as *marks*.

Common choices of marks include the event's magnitude, duration and spatial location, with values over a measurable space  $\mathbb{M}$ . (Marked) Hawkes processes are a class of (marked) point processes which exhibit a *self-exciting behavior*, meaning that the occurrence of an event can lead to the occurrence of additional, subsequent events. A marked point process  $X$  gives rise to marked point patterns of the form  $\mathbf{x} = \{(t_i, \kappa_i)\}$ , where  $t_i \in \mathbb{R}$  and  $\kappa_i \in \mathbb{M}$  denote the time and mark of the  $i^{\text{th}}$  event. Let  $N$  be the corresponding counting measure for the process on  $\mathbb{R}$  which counts the number of points falling within any arbitrary Borel set. Also, let  $\mathcal{H}_t$  denote the process' history up to time  $t$ ,  $\mathcal{H}_t = \{(t_i, \kappa_i) \text{ such that } t_i < t\}$ . The process' mechanisms are often characterized through its (conditional) intensity, defined as the limit of the expected number of points in an infinitesimal time window following  $t$  given the realized history  $\mathcal{H}_t$  (Daryl and Vere-Jones, 2003),

$$\lambda^*(t) = \lim_{\Delta t \downarrow 0} \frac{\mathbb{E}[N\{(t, t + \Delta t)\} \mid \mathcal{H}_t]}{\Delta t}.$$

For the marked Hawkes process, the conditional intensity is of the form

$$\lambda^*(t) = \mu(t) + \sum_{(t_i, \kappa_i) \in \mathcal{H}_t} \alpha(\kappa_i) \beta(t - t_i, \kappa_i), \quad (1)$$

and the corresponding mark distribution is

$$\gamma^*(\kappa|t) = \gamma(\kappa|t, \mathcal{H}_t),$$

which describes the mechanism that assigns marks to future events. The superscript  $*$  is used in both cases to denote that the functions are defined conditional on the history. The functions in (1) satisfy that  $\mu(\cdot)$  is a non-negative function on  $\mathbb{R}$ ,  $\alpha(\cdot)$  is a non-negative function on  $\mathbb{M}$  and  $\beta(\cdot, \kappa)$  is a density function on  $[0, \infty)$  which is allowed to depend on  $\kappa$ . Since we mainly focus on the spatio-temporal Hawkes processes in this manuscript,  $\kappa$  is thought to represent an event's spatial coordinates.

An alternative formalization of the Hawkes process that will be useful moving forward views the Hawkes process as a Poisson cluster process (Hawkes and Oakes, 1974). From this point of view, an event is either an immigrant that occurred in the system separately from previous events, or an offspring of a previous event

which occurred due to the process' self-excitement. The set of these relations is called the process' branching structure. We denote event  $j$ 's (latent) branching information as  $Y_j$ , where  $Y_j = 0$  if  $t_j$  is an immigrant and  $Y_j = i$  if  $t_j$  is an offspring of event  $i$ . The collection of this information across all events is denoted by  $\mathbf{Y}$ . Under the Poisson clustering representation of the Hawkes process, a realization of the process can be thought of as occurring in the following manner. First, the set of all immigrants  $I = \{t_i : Y_i = 0\}$  (or "generation 0") are generated from a marked Poisson process with  $\lambda_I(t) = \mu(t)$  and the associated mark density  $\gamma_I(\kappa|t) = \gamma(\kappa|t)$ . Then, each of the immigrant events  $t_i \in I$  can give rise to offspring events  $O_i = \{t_j : Y_j = i\}$  in generation 1. Events in  $O_i$  are generated as a marked Poisson process with intensity  $\lambda_{O_i}(t) = \alpha(\kappa_i)\beta(t - t_i, \kappa_i)$  and mark density  $\gamma_{O_i}(\kappa|t) = \gamma(\kappa|t, (t_i, \kappa_i))$ . At the next step, each event in generation 1 could lead to events in generation 2 in the same manner, and that continues on. Due to this representation,  $\mu(t)$  and  $\alpha(\kappa)\beta(t, \kappa)$  are called background intensity and offspring intensity, respectively. This representation also illustrates that  $\alpha(\kappa)$  represents the mean number of offsprings of an event with mark  $\kappa$ , and  $\beta(\cdot, \kappa)$  is the density function of the length of time interval between an offspring and its parent.

For our discussion in Section 3, it is useful to introduce the likelihood of an observed marked point pattern  $\mathbf{x}$  during a time period  $[0, T)$  under the Hawkes model. If  $\theta$  is the vector of all parameters, then conditional on the branching structure

$$\begin{aligned}
p(\mathbf{x}|\mathbf{Y}, \theta) &= p(I|\mathbf{Y}, \theta) \prod_{i=1}^n p(O_i|\mathbf{Y}, \theta) \\
&= \exp(-M(T)) \prod_{t_i \in I} \mu(t_i) \gamma(\kappa_i|t_i) \\
&\quad \times \prod_{i=1}^n \left\{ \exp(-\alpha(\kappa_i)B(T - t_i, \kappa_i)) \prod_{t_j \in O_i} \alpha(\kappa_i) \beta(t_j - t_i, \kappa_i) \gamma(\kappa_j|t_j, (t_i, \kappa_i)) \right\},
\end{aligned} \tag{2}$$

where  $M(T) = \int_0^T \mu(t) dt$ , and  $B(T - t_i, \kappa_i) = \int_0^{T-t_i} \beta(t, \kappa_i) dt$ .

## 2.2 Multivariate Hawkes process

The Hawkes processes has been extended to accommodate multiple processes with mutually-exciting behavior. An  $L$ -dimensional marked process gives rise to point patterns of the form  $\{(t_{l,i}, \kappa_{l,i}) : l \in \{1, \dots, L\}, i \in \mathbb{N}\}$ , where  $t_{l,i}$  and  $\kappa_{l,i}$  are the time and marks of the  $i^{th}$  event from process  $l$ . The multivariate Hawkes

process can be defined through the respective conditional intensity of each of its  $L$  components:

$$\lambda_l^*(t) = \mu_l(t) + \sum_{m=1}^L \sum_{t_{l,i} < t} \alpha_{m,l}(\kappa_{l,i}) \beta_{m,l}(t - t_{l,i}, \kappa_{l,i}), \quad (3)$$

where  $l = 1, 2, \dots, L$ , and (implicitly) the history is now extended to include times and marks for the events occurring before time  $t$  from *all*  $L$  processes. Similar to the univariate case, a multivariate Hawkes process can be viewed as a Poisson cluster process generated by a latent branching structure  $\mathbf{Y} = \{Y_{l,i}\}$  where  $Y_{l,j} = (0, 0)$  if  $t_{l,j}$  is an immigrant and  $Y_{l,j} = (k, i)$  if  $t_{l,j}$  is an offspring of  $t_{k,i}$ . Through this equivalence, we can conceive  $\mu_l(t)$  as the background intensity for process  $l$  and  $\alpha_{m,l}(\kappa_{l,i}) \beta_{m,l}(t - t_{l,i}, \kappa_{l,i})$  as the offspring intensity corresponding to either self-excitation ( $m = l$ ) or external-excitation ( $m \neq l$ ).

### 3 Aggregated Hawkes process

Standard estimation techniques for the parameters of the Hawkes process require that the available data include exact information on the time and characteristics of the events. However, in many situations researchers only have access to some limited information about the events: they might know the date or region an event occurred, without having access to its precise time stamp or location. We refer to such data as “aggregated” point pattern data, and we consider estimation of parameters of the underlying process when the underlying exact event occurrence follows a Hawkes process.

In this section, we introduce a Bayesian approach for estimating the parameters in spatio-temporal Hawkes processes when aggregation occur over time, space, or both. In Section 3.2, we develop the sampling scheme based on latent variables. We introduce the models that we consider in Section 3.3 and give details about the MCMC steps in Section 3.4.

#### 3.1 Aggregated event information

We consider three scenarios of aggregated data from Hawkes processes of increasing complexity. Aggregated temporal event data, aggregated spatio-temporal event data, and the scenario with aggregated event data on multiple processes. We assume that the process is observed during the  $[0, T]$  time window, and over a spatial window  $W = [0, W_x] \times [0, W_y]$ . We consider a rectangular spatial window here for notational simplicity,

though our approach could be applied to spatial windows of any shape.

For aggregated temporal data, the time interval  $[0, T]$  is partitioned into  $n_1$  bins  $B_1^t, B_2^t, \dots, B_{n_1}^t$ . Then, the observed data correspond to the number of events that occurred within each temporal bin, denoted by  $N_1, N_2, \dots, N_{n_1} \in \{0\} \cup \mathbb{Z}^+$ . For aggregated spatio-temporal data, the spatial window is also partitioned in  $n_2$  bins,  $B_1^\kappa, B_2^\kappa, \dots, B_{n_2}^\kappa$ . In this case, the observed data are of the form  $\{N_{i,j} : i = 1, \dots, n_1, j = 1, \dots, n_2\}$ , where  $N_{i,j}$  denotes the number of events in  $B_i^t \times B_j^\kappa$ . We consider temporal bins of equal size  $\Delta^t$ , and that the spatial marks are aggregated on a grid sharing the same length  $\Delta^\kappa$ . Therefore, in what follows we have  $B_i^t = [(i-1)\Delta^t, i\Delta^t)$  and  $B_j^\kappa$  is of the form  $[(k-1)\Delta^\kappa, k\Delta^\kappa) \times [(m-1)\Delta^\kappa, m\Delta^\kappa)$  for some  $k, m \in \mathbb{N}$ . We refer to  $\Delta^t$  and  $\Delta^\kappa$  as the size of aggregation in time and space, respectively. A visualization of aggregated spatio-temporal data is shown in Figure 1. We maintain time and space bins of equal size for notational simplicity, though we note here that it is easy to modify our approach for more complicated settings with unequal bin lengths in time or irregular shapes in space.

When there are  $L$  processes, the aggregation sizes in time and space for each process may be different. We denote the aggregation sizes in time and space for process  $l$  by  $\Delta_l^t$  and  $\Delta_l^\kappa$ , respectively, and the spatio-temporal bins by  $B_{l,i}^t \times B_{l,j}^\kappa : i = 1, \dots, n_{l,1}, j = 1, \dots, n_{l,2}$ . Then the aggregated data for multiple processes are in the form  $\{N_{l,i,j} : l = 1, \dots, L, i = 1, \dots, n_{l,1}, j = 1, \dots, n_{l,2}\}$  where  $N_{l,i,j}$  is the number of events from process  $l$  in  $B_{l,i}^t \times B_{l,j}^\kappa$ .

### 3.2 Latent variable formulation

Even though available data are in aggregated form, the events truly occur in continuous time and space, and ignoring dependencies among events in the same bin can lead to misleading conclusions. Instead our approach models the aggregated event data at the scale they actually occur. We consider the exact time and location of an event as latent variables, and we formalize an approach to estimate the parameters of a continuous time and space Hawkes process using the available aggregated data. Below, we introduce our approach for a single aggregated spatio-temporal process. This formulation is simplified in the case of a temporal process, and extended in the case of multiple spatio-temporal processes, though we refrain from presenting the details here (we refer interested readers to Appendix B.1).

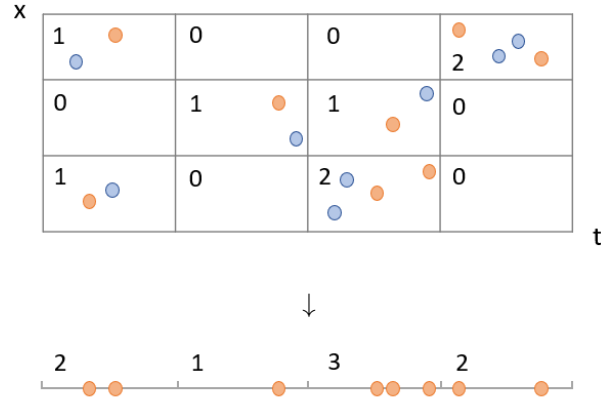


**Figure 1:** Exact and Aggregated Point Pattern Data. The continuous time (horizontal axis) is divided in four time bins, and the continuous space (one-dimensional, vertical axis) is divided in three bins. The data might be available with spatial information on the  $3 \times 4$  spatio-temporal bins (top), and without spatial information on the 4 temporal bins (bottom). The orange points represent the exact spatio-temporal data. Then, the available aggregated data correspond to the count of events occurring within each bin. The blue points represent an alternative point pattern that would match the same aggregated data.

Let  $\mathbf{N} = \{N_{i,j} : i = 1, \dots, n_1, j = 1, \dots, n_2\}$  be the aggregated data, and  $\mathbf{x} = \{(t_i, \kappa_i) : i = 1, \dots, n\}$  be the underlying exact point pattern which is unobserved. We propose a Bayesian approach to estimate the parameters of the Hawkes process ( $\theta$ ) which integrates over the distribution of the latent exact point pattern  $\mathbf{x}$  and its latent branching structure  $\mathbf{Y}$  (discussed in Section 2). We write the likelihood of the observed data given the parameters of the Hawkes process as

$$p(\mathbf{N} | \theta) = \int p(\mathbf{N}, \mathbf{x}, \mathbf{Y} | \theta) d\mathbf{x} d\mathbf{Y}$$

and note that

$$p(\mathbf{N}, \mathbf{x}, \mathbf{Y} | \theta) = p(\mathbf{N} | \mathbf{x}, \mathbf{Y}, \theta) p(\mathbf{x} | \mathbf{Y}, \theta) p(\mathbf{Y} | \theta).$$

Given the exact point pattern  $\mathbf{x}$ , the distribution of the aggregated data  $p(\mathbf{N} | \mathbf{x}, \mathbf{Y}, \theta)$  is equal to 1 only when the aggregated data match the exact point pattern in terms of the total number of events  $\sum_{i=1}^{n_1} \sum_{j=1}^{n_2} N_{i,j} = n$ , and the number of events by bin,  $\sum_{k=1}^n 1\{(t_k, \kappa_k) \in B_i^t \times B_j^\kappa\} = N_{i,j}$  for all  $i, j$ . Figure 1 shows two exact point patterns that lead to the same aggregated data. Given the branching structure and the Hawkes parameters, the exact point pattern follows the distribution given in (2).



Assuming a prior on the model parameters  $p(\theta)$  (which will be discussed in Section 3.4), the posterior distribution of the model parameters  $p(\theta | \mathbf{N})$  is acquired by integrating out the exact Hawkes point pattern and corresponding branching structure from their joint posterior distribution  $p(\mathbf{x}, \mathbf{Y}, \theta | \mathbf{N})$ . Therefore, we approximate the joint posterior distribution of  $(\mathbf{x}, \mathbf{Y}, \theta)$  using MCMC methods and discard samples of  $(\mathbf{x}, \mathbf{Y})$ . We do so by iteratively sampling from (1)  $p(\mathbf{x} | \mathbf{N}, \mathbf{Y}, \theta)$ , and (2)  $p(\theta, \mathbf{Y} | \mathbf{N}, \mathbf{x})$ . In Step (1) an exact point pattern is drawn from its conditional posterior distribution, such that the drawn point pattern agrees with the aggregated observed data  $\mathbf{N}$ . Then, since  $p(\theta, \mathbf{Y} | \mathbf{N}, \mathbf{x}) = p(\theta, \mathbf{Y} | \mathbf{x})$ , Step (2) can be performed as if the exact point pattern had been observed. We discuss how Step (1) can be efficiently performed along with a more detailed description of the MCMC steps in Section 3.4. Bayesian approaches that augment their sampling scheme using latent variables in an iterative manner are commonly used in modeling event occurrence (e.g., Tucker *et al.*, 2019; Bu *et al.*, 2022) in the presence of missing or aggregate data.

### 3.3 Parametric specifications of the Hawkes model

In the case of temporal data, spatio-temporal data, and data on multiple processes, we focus on specifications of the Hawkes model which are commonly found in the literature.

First, we specify that the occurrence of immigrants is homogeneous in time by specifying  $\mu(t) = \mu 1\{t \geq 0\}$ . We also assume that the time from a parent to an offspring follows an exponential decay offspring density  $\beta(t) = \beta \exp(-\beta t)$  (with mean  $1/\beta$ ). For spatio-temporal data (i.e  $\kappa$  is the spatial coordinates of the event),  $\mu(t)$  and  $\beta(t)$  are specified in the same manner, and we assume a constant expected number of offsprings across space,  $\alpha(\kappa) = \alpha$ . The location of immigrant events is assumed to arise from a uniform distribution over the region  $W$  (extended in Section 5), and the location of an event's offspring is assumed to be generated from a bivariate normal distribution centered at the location of the parent. These specifications correspond to  $\gamma_I(\kappa | t) = \frac{1\{\kappa \in W\}}{|W|}$  and  $\gamma_O(\kappa | t, (t_{pa}, \kappa_{pa})) = (2\pi\gamma^2)^{-1/2} \exp\left(-\frac{\|\kappa - \kappa_{pa}\|^2}{2\gamma^2}\right)$ , where  $|W|$  is the area of the spatial window and  $\|\cdot\|$  denotes the  $l^2$ -norm.

Lastly, in the case of  $L$  mutually exciting processes, the specifications above are maintained while allowing for different parameters for each of the process. If  $l, m \in \{1, 2, \dots, L\}$  is used to denote any two processes, the immigrant intensity is homogeneous in time,  $\mu_l(t) = \mu_l 1\{t \geq 0\}$ , and the spatial distribution of the

immigrant events is a uniform over the region  $W$ ,  $\gamma_I(\kappa | t) = \frac{1\{\kappa \in W\}}{|W|}$ . The model incorporates cross-excitement by specifying functions  $\alpha, \beta$  and  $\gamma$  for all  $(l, m)$  pairs. We assume that the expected number of offsprings is constant for parent events in any location, while allowing it to be different across  $(l, m)$  combinations,  $\alpha_{m,l}(\kappa_{l,i}) = \alpha_{m,l}$ . Similarly, we maintain that the time from parent to offspring follows an exponential distribution, and the location of an offspring event is normally distributed around the location of its parent event,  $\beta_{m,l}(t) = \beta_{m,l} \exp(-\beta_{m,l}t)$ , and  $\gamma_{m,l}(\kappa | (t_{pa}, \kappa_{pa})) = (2\pi\gamma_{m,l}^2)^{-1/2} \exp\left(-\frac{\|\kappa - \kappa_{pa}\|^2}{2\gamma_{m,l}^2}\right)$ .

Hawkes process models are flexible and there are many other choices for  $\mu(t)$ ,  $\alpha(\kappa)$ ,  $\beta(t)$ ,  $\gamma_I(\kappa|t)$  and  $\gamma_O(\kappa|t, (t_{pa}, \kappa_{pa}))$ . Most parametric alternatives are straightforward to implement within our framework. A variation of the spatio-temporal model that does not assume a uniform density for the location of the immigrants is used in Section 5.

### 3.4 Estimation and inference within the Bayesian framework

We return to the case of spatio-temporal aggregated data discussed in Section 3.2, where the observed data are in the form  $\mathbf{N} = \{N_{i,j} : i = 1, \dots, n_1, j = 1, \dots, n_2\}$  and  $\mathbf{x} = \{(t_i, \kappa_i) : i = 1, \dots, n\}$  denotes the exact data on  $[0, T] \times W$ . Even though the details presented here correspond to the spatio-temporal case, they apply to the temporal Hawkes process, or extend to mutually-exciting spatio-temporal Hawkes processes (see Appendix B.2 for details).

We adopt (independent) gamma priors for  $\mu, \alpha$  and  $\beta$ , and an inverse gamma prior for  $\gamma^2$ :

$$\mu \sim \text{Gamma}(a_1, b_1), \alpha \sim \text{Gamma}(a_2, b_2), \beta \sim \text{Gamma}(a_3, b_3), \gamma^2 \sim \text{IG}(a_4, b_4),$$

where the second number in the gamma distribution denotes the rate parameter. Throughout the paper, we choose  $a_1 = a_2 = 1$  and  $b_1 = b_2 = 0.01$  for the priors on  $\mu$  and  $\alpha$ , and  $a_4 = b_4 = 0.001$  for the prior on  $\gamma^2$ . We set  $a_3 = 1$  and take  $b_3 = 0.01$  for the simulations and  $b_3 = 1$  for our study (see Section 5 for this choice). We specify a prior distribution for the branching structure recursively (Tucker *et al.*, 2019). For  $i = 1, 2, \dots, n$ , we assume a discrete uniform distribution on feasible values of  $Y_i$ , i.e.  $Y_i \sim \text{Unif}(\{0, 1, \dots, i-1\})$ .

Given the latent branching structure and the model parameters, the exact data are assumed to follow

the distribution specified in (2), which under the parametric specifications in Section 3.3 becomes

$$p(\mathbf{x}|\mathbf{Y}, \theta) = \exp(-\mu T)(\mu|W|^{-1})^{|I|} \times \prod_{i=1}^n \left\{ \exp \left\{ -\alpha \{1 - \exp[-\beta(T - t_i)]\} \right\} \prod_{t_j \in O_i} \frac{\alpha\beta}{\sqrt{2\pi\gamma^2}} \exp \left[ -\beta(t_j - t_i) - \frac{\|\kappa_j - \kappa_i\|^2}{2\gamma^2} \right] \right\} \quad (4)$$

where  $|I|$  denotes the number of immigrants. Then, conditional on the latent exact data, the distribution of the aggregated data is

$$p(\mathbf{N}|\mathbf{x}, \theta, \mathbf{Y}) = \begin{cases} 1 & \text{if } \sum_{k=1}^n 1\{(t_k, \kappa_k) \in B_i^t \times B_j^\kappa\} = N_{i,j} \text{ for all } i, j, \quad \text{and} \\ 0 & \text{otherwise} \end{cases}$$

We approximate the posterior distribution of all parameters and latent variables using MCMC. We use Gibbs sampling for parameters  $\mu, \alpha$ , and  $\gamma$ , and for the latent branching structure  $\mathbf{Y} = (Y_1, Y_2, \dots, Y_n)$ . Specifically, we iteratively sample from

$$\begin{aligned} \mu|\mathbf{x}, \theta_{-\mu}, \mathbf{Y}, \mathbf{N} &\sim \text{Gamma}(a_1 + |I|, b_1 + T) \\ \alpha|\mathbf{x}, \theta_{-\alpha}, \mathbf{Y}, \mathbf{N} &\sim \text{Gamma}(a_2 + \sum_{i=1}^n |O_i|, b_2 + \sum_{i=1}^n \beta \exp(-\beta(T - t_i))) \\ \gamma^2|\mathbf{x}, \theta_{-\gamma}, \mathbf{Y}, \mathbf{N} &\sim \text{IG}(a_4 + \sum_{i=1}^n |O_i|, b_4 + \frac{1}{2} \sum_{i=1}^n \sum_{t_j \in O_i} \|\kappa_j - \kappa_i\|^2), \end{aligned}$$

where  $\theta = (\mu, \alpha, \beta, \gamma)$  and  $\theta_{-(\cdot)}$  excludes the one in the subscript. The full conditional of  $Y_i$  is a multinomial distribution given by

$$P(Y_i = j | \theta, \mathbf{Y}) \propto \begin{cases} \mu|W|^{-1}, & \text{for } j = 0, \quad \text{and} \\ \frac{\alpha\beta}{\sqrt{2\pi\gamma^2}} \exp \left( -\beta(t_i - t_j) - \frac{\|\kappa_i - \kappa_j\|^2}{2\gamma^2} \right), & \text{for } j = 1, 2, \dots, i-1. \end{cases}$$

To improve the computational efficiency of the algorithm, we avoid evaluating the conditional probability above potential parent events  $j$  that precede event  $i$  by an unrealistically long amount of time. We do so by truncating this multinomial distribution to events  $j$  for which  $(t_i - t_j)$  is below the 99+<sup>th</sup> quantile of the Exponential( $\beta$ ) distribution.

There are no conjugate priors for  $\beta$ . Therefore, we use Metropolis-Hasting to sample from its full conditionals. Specifically, we propose value  $\beta'$  from a normal distribution with mean  $\beta^c$  and standard deviation  $\sigma_\beta$ , where superscripts  $c$  denotes the current value and  $'$  denotes the proposed value. We accept the move with probability

$$H_\beta = \min \left( 1, \left( \frac{\beta'}{\beta^c} \right)^{a_3-1} \exp(b_3(\beta^c - \beta')) \prod_{i=1}^n \left\{ \exp \left( \alpha \exp(-\beta'(T - t_i)) - \alpha \exp(-\beta^c(T - t_i)) \right) \right. \right. \\ \left. \left. \times \prod_{j \in \mathcal{O}_i} \frac{\beta'}{\beta^c} \exp \left( -(\beta' - \beta^c)(t_j - t_i) \right) \right\} \right)$$

Lastly, sampling the latent exact data  $\mathbf{x}$  has to be performed such that they match the aggregated data  $\mathbf{N}$ . We decompose  $\mathbf{x}$  to  $(\mathbf{t}, \boldsymbol{\kappa})$  for  $\mathbf{t} = (t_1, t_2, \dots, t_n)$  and  $\boldsymbol{\kappa} = (\kappa_1, \kappa_2, \dots, \kappa_n)$ , and perform element-wise Metropolis-Hastings while ensuring that the observed data constraints are satisfied. For  $i = 1, 2, \dots, n$ ,  $t'_i$  is drawn from a continuous uniform distribution that satisfies the following restrictions:  $t'_i$  is within the time bin of event  $i$ , it occurs after its parent event (if it has one,  $Y_i \neq 0$ ), and before its offsprings (if any). The proposed value of  $t_i$  is accepted with probability

$$H_{t_i} = \min \left( 1, \exp \left( \alpha \beta \exp(-\beta(T - t_i^c)) - \alpha \beta \exp(-\beta(T - t'_i)) \right) - (|\mathcal{O}_i| + 1\{Y_i > 0\})\beta(t'_i - t_i^c) \right).$$

Similarly,  $\kappa_i$  is drawn from a uniform distribution on the space bin containing  $\kappa_i$  and the proposed move is accepted with probability

$$H_{\kappa_i} = \min \left( 1, \exp \left( \frac{-\|\kappa'_i - \kappa_{\text{pa}}\|^2 + \|\kappa_i^c - \kappa_{\text{pa}}\|^2}{2\gamma^2} 1\{Y_i > 0\} + \sum_{j \in \mathcal{O}_i} \frac{-\|\kappa'_i - \kappa_j\|^2 + \|\kappa_i^c - \kappa_j\|^2}{2\gamma^2} \right) \right)$$

It is possible to update  $t_1, t_2, \dots, t_n$ , or  $\kappa_1, \kappa_2, \dots, \kappa_n$  simultaneously, though designing reasonable proposal distributions with admissible acceptance rates for simultaneous updates is challenging. We find that updating these parameters one at a time is easy to implement, computationally fast, and that the proposed MCMC algorithm performed well in the simulations and the application we considered, with minimal tuning.

## 4 Simulations

We investigate the performance of our method on simulated data in different scenarios. Particularly, we explore the effect that fine or coarse aggregations of time and space have on the method’s performance. We focus on the univariate temporal case in Section 4.1 and the spatio-temporal case in Section 4.2. Then, we turn our attention to the case of multivariate spatio-temporal data in Section 4.3. For each setting, we simulate data from a Hawkes process in continuous time and space and aggregate them in pre-defined bins.

### 4.1 Temporal simulations

In this section, we consider estimation of the parameters of the Hawkes process based on aggregated temporal data. Data for the temporal and spatio-temporal simulations were generated simultaneously. We simulate data sets from a Hawkes process on a time window  $[0, 500]$  and a spatial window  $[0, 100] \times [0, 100]$  using two parameter sets:

1.  $(\mu, \alpha, \beta, \gamma) = (0.3, 0.7, 1, 1)$
2.  $(\mu, \alpha, \beta, \gamma) = (0.5, 0.5, 1, 1)$

Data sets generated by these two parameter sets have similar total number of events but the process produces fewer immigrants and more offsprings under parameter set 1 than under 2. Since the conditional intensity  $\lambda^*(t)$  in the data generative model does not depend on the spatial marks, we simply ignored the spatial information for performing the temporal simulations. For each parameter set, we simulate 400 data sets.

For our simulations, we consider time aggregations in terms of the true value of  $1/\beta$ , which is the expected length of time between an offspring and its parent. We consider aggregated data in bins of length  $\Delta^t = 0, 0.5, 0.75, 1, 1.25, 1.5$  (times  $1/\beta$ ), where  $\Delta^t = 0$  indicates that there is no aggregation. We consider the performance of the proposed Bayesian method, and the frequentist MC-EM approach proposed by Shlomovich *et al.* (2022). For each data set, we fit the Hawkes model using the exact data which is used as the “gold standard” approach. Then, we fit both methods on the aggregated data of all levels of coarseness.

First, we investigate how results from our model that uses aggregated data compare to the results one would acquire had they had access to the exact data ( $\Delta^t = 0$ ). Table 1 shows the average estimate

**Table 1:** Results of the temporal simulation. The table shows the average posterior mean (“Estimate”), average 95% credible interval length (“CI length”), and coverage rate of the 95% credible interval (“Coverage”) for parameters  $\mu$ ,  $\alpha$  and  $\beta$  of the Hawkes process, across 400 simulated data sets, for the exact data ( $\Delta^t = 0$ ), temporal aggregations of different sizes, and two sets of parameters. 95% credible interval is determined by the 2.5 and 97.5 quantiles of the posterior samples.

		Parameter set 1				Parameter set 2			
	$\Delta^t$	Estimate	CI length	Coverage		$\Delta^t$	Estimate	CI length	Coverage
$\mu$	0	0.3105	0.1674	0.9275	$\mu$	0	0.5141	0.2421	0.9575
	0.5	0.3110	0.1678	0.9325		0.5	0.5149	0.2436	0.9625
	0.75	0.3113	0.1682	0.9375		0.75	0.5156	0.2446	0.9550
	1	0.3116	0.1688	0.9375		1	0.5166	0.2456	0.9475
	1.25	0.3117	0.1696	0.9300		1.25	0.5161	0.2473	0.960
	1.5	0.3121	0.1701	0.930		1.5	0.5178	0.2491	0.9449
	$\alpha$	0	0.6802	0.2057		0.9200	$\alpha$	0	0.4829
0.5		0.6797	0.2061	0.9225	0.5	0.4820		0.2457	0.9500
0.75		0.6795	0.2064	0.9250	0.75	0.4814		0.2466	0.9325
1		0.6789	0.2070	0.9325	1	0.4802		0.2475	0.9350
1.25		0.6790	0.2077	0.9225	1.25	0.4809		0.2493	0.950
1.5		0.6785	0.2080	0.920	1.5	0.4792		0.2509	0.9273
$\beta$		0	1.0441	0.6090	0.9450	$\beta$		0	1.0909
	0.5	1.0489	0.6288	0.9475	0.5		1.1072	1.0630	0.9500
	0.75	1.0542	0.6491	0.9525	0.75		1.1238	1.1416	0.9475
	1	1.0615	0.6793	0.9475	1		1.1667	1.3206	0.9275
	1.25	1.0663	0.7061	0.9575	1.25		1.1796	1.4213	0.935
	1.5	1.0713	0.7334	0.945	1.5		1.2319	1.7509	0.9449

(posterior mean), average length of 95% credible interval, and coverage rate for each parameter under the different aggregations. For both parameter sets, the estimates and credible interval lengths for  $\mu$  and  $\alpha$  are largely unaffected by the data’s temporal aggregation. On the other hand, the credible interval length for  $\beta$  is on average wider, and the estimate of  $\beta$  is on average larger for coarser temporal aggregations. The efficiency loss in estimating  $\beta$  is expected for larger aggregations, since  $1/\beta$  is the expected time from parent to offspring, and temporal aggregation would result to parent-offspring pairs within the same temporal bin. The coarseness of the temporal aggregation has a larger effect for  $\beta$  under the parameter set 2. This is also expected as data sets generated by parameter set 2 contain a smaller ratio of offsprings, and for that reason, the aggregation will lead to even fewer parent-offspring pairs in separate bins, and high uncertainty in learning the events’ branching structure. The efficiency loss with larger temporal aggregations is alleviated in the presence of spatial information, as we illustrate in Section 4.2.

We compare the performance of our Bayesian method with the MC-EM method on the same data sets. We focus first on results from parameter set 1. In three simulated data sets, MC-EM did not converge and

the corresponding estimates were removed. Figure 2 shows boxplots for the estimates of  $\mu$ ,  $\alpha$  and  $\beta$  for both methods and different aggregations  $\Delta^t$ , under parameter set 1. The true parameter values are indicated by the red line. Both methods are essentially unbiased. The Monte Carlo variance for estimating  $\mu$  and  $\beta$  is similar for the two methods, but the Monte Carlo variability for  $\alpha$  is lower based on our Bayesian method than when using the MC-EM method. The performance of the MC-EM algorithm *deteriorates significantly* under parameter set 2 and large aggregations. Results from MC-EM are unstable, the MC-EM method did not converge for 234 out of 400 simulated data sets, and yielded unreasonably large estimates when  $\Delta^t = 1.5$  (see Figure A.1).

In our temporal simulations, we find that the proposed Bayesian approach has accuracy gains in terms of estimation of  $\alpha$ , and is stable across all aggregations. Moreover, it offers a straightforward inference procedure. In contrast, the MC-EM approach does not offer a way for inference, and it is only applicable for temporal Hawkes process (no marks). Therefore, the MC-EM algorithm cannot be applied in the remaining simulations in this section.

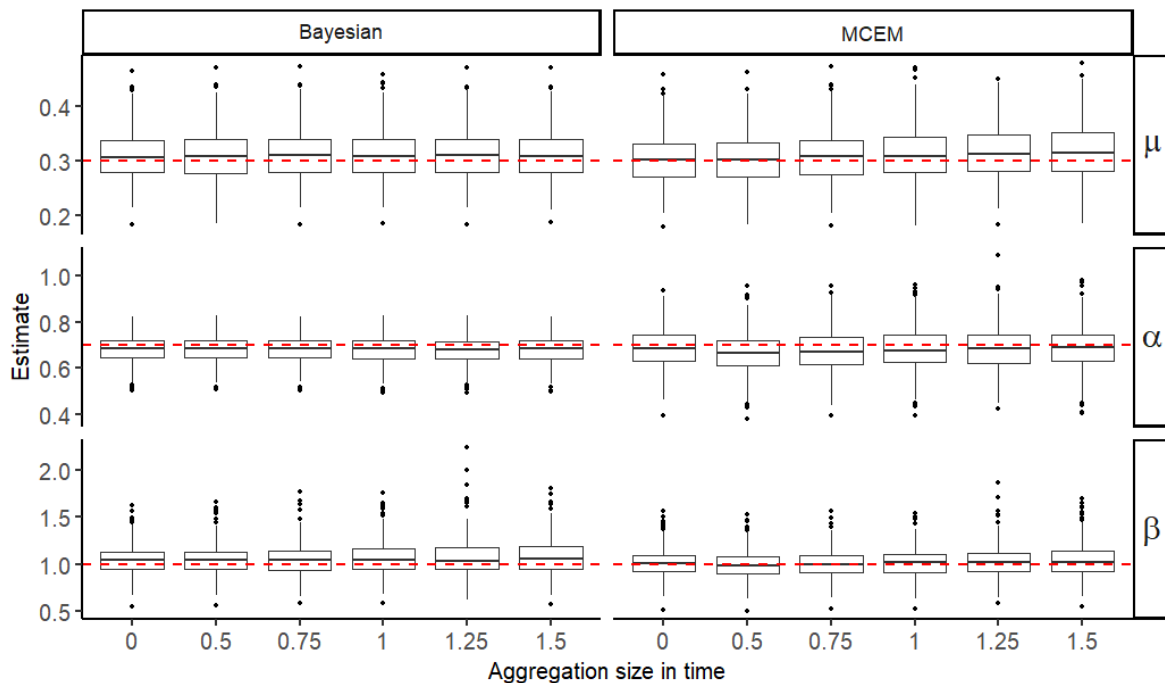


**Figure 2:** Boxplot for the estimates of  $\mu$ ,  $\alpha$  and  $\beta$  using our Bayesian approach (left) and the MC-EM approach (right). The horizontal red lines indicate the true values which correspond to parameter set 1:  $(\mu, \alpha, \beta) = (0.3, 0.7, 1)$ . Results for parameter set 2 are shown in Figure A.1.

## 4.2 Spatio-temporal simulations

We use data sets simulated in Section 4.1 for the parameter set 1 as exact data. Based on the true values of  $\beta$  and  $\gamma$ , we choose to aggregate the data with  $\Delta^t = 0, 0.5, 1, 1.5$  (times  $1/\beta$ ) and  $\Delta^s = 0, 0.5, 1, 1.5$  (times  $\gamma$ ). We summarize the findings here, and we present the full results of the spatio-temporal simulation in Table A.2. Similar analysis is also conducted for simulations for parameter set 2, and the full results are included in Table A.3. Across all aggregations over time and space we considered, we found that the bias was negligible. Specifically, the bias ranges from -0.0118 to 0.0295 across all scenarios considered and all parameters. Similarly, coverage varies from 92.5 to 96% with most values close to 95%. Similar to the temporal case, we find that the uncertainty with regards to estimation of  $\mu$  and  $\alpha$  does not change much as the aggregation in time and space becomes coarser. Therefore, we focus on the parameters  $\beta, \gamma$ . Figure 3 shows the mean length of 95% credible intervals for  $\beta$  and  $\gamma$  when data is aggregated in time and space with different aggregation sizes. Even though aggregation in time and space affect the credible interval lengths for both  $\beta$  and  $\gamma$ , the credible interval lengths of  $\beta$  are mainly influenced by time aggregation, while the credible interval lengths of  $\gamma$  are mainly influenced by space aggregation.

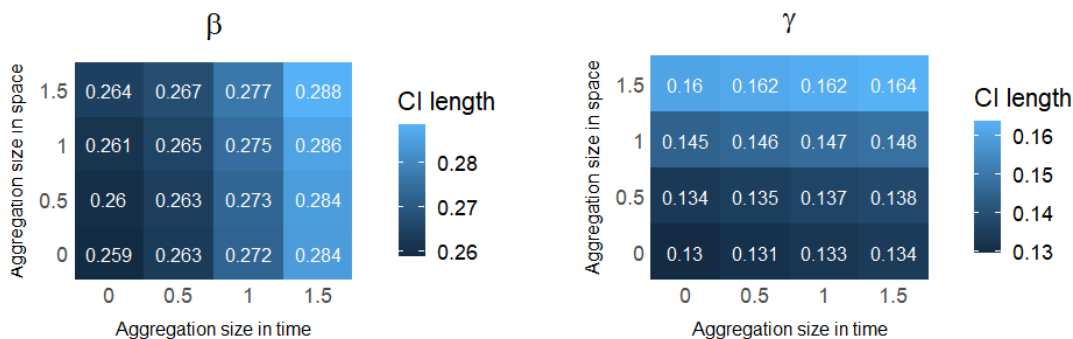


**Figure 3:** Average credible interval length for  $\beta$  and  $\gamma$  over 400 simulated spatio-temporal data sets and based on different aggregation sizes in time and space.

Lastly, we compared the results from the temporal model (which ignores spatial marks – Table 1) and the spatio-temporal model (Tables A.2 and A.3) based on varying aggregation sizes. Incorporating the spatial marks leads to a reduction in bias and coverage closer to the nominal level, irrespective of the size of the time and space aggregation. In fact, the bias and efficiency loss observed for  $\beta$  under large temporal aggregations in parameter set 2 (Section 4.1) is almost entirely mitigated when spatial information is available, even



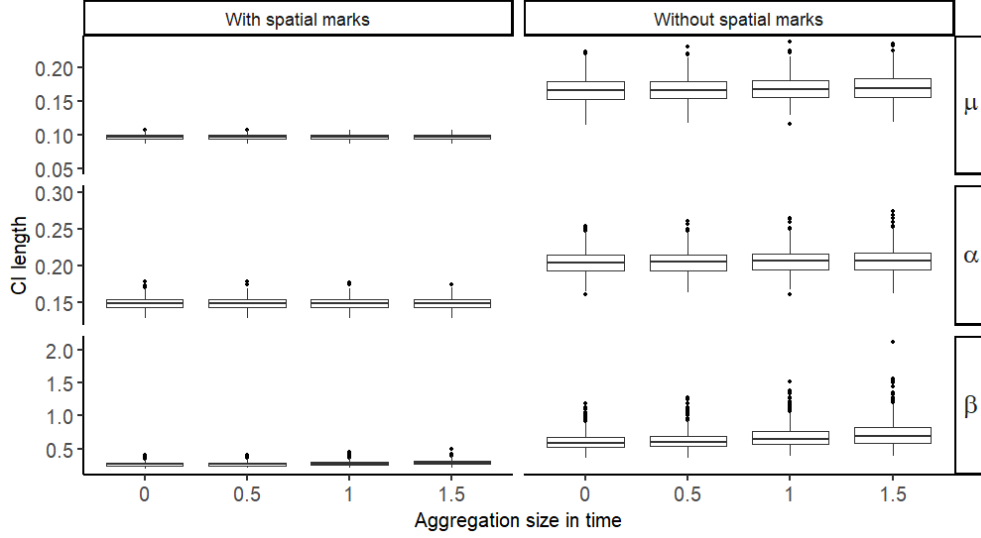


**Figure 4:** Credible Interval Lengths from the Temporal and Spatio-temporal Models. Boxplots of the 95% credible interval for  $\mu$ ,  $\alpha$ , and  $\beta$  across 400 simulated data sets, for varying temporal aggregations  $\Delta^t = 0, 0.5, 1, 1.5$  (horizontal axis) and coarse spatial aggregation  $\Delta^\kappa = 1.5$ .

at coarse spatial bins. In terms of estimation efficiency, Figure 4 illustrates the CI length of the models' common parameters  $\mu$ ,  $\alpha$ ,  $\beta$  across the simulated data sets with  $\Delta^t = 0, 0.5, 1, 1.5$  and the coarsest space aggregation  $\Delta^\kappa = 1.5$ . Even with coarsely aggregated spatial marks, the CI lengths of all parameters are much smaller based on the spatio-temporal model than based on the temporal model. This is true even when the event times are known exactly ( $\Delta^t = 0$ ). These results indicate that, if spatial information is available, incorporating it leads to more accurate estimation of the model parameters for the underlying Hawkes process, even when the location of the events is known at coarse levels. Our approach provides a framework to incorporate such coarse spatial information in the estimation procedure, and improve estimation efficiency. For finer space aggregations  $\Delta^\kappa < 1.5$ , the CI length reduction when incorporating spatial marks is similar.

### 4.3 Simulations on multiple spatio-temporal processes

We simulate 400 data sets from a bivariate Hawkes process on the time window  $[0, 500]$  and the spatial window  $[0, 100] \times [0, 100]$ , using parameters

$$\mu = \begin{pmatrix} 0.3 \\ 0.5 \end{pmatrix}, \quad \alpha = \begin{pmatrix} 0.7 & 0.15 \\ 0.3 & 0.5 \end{pmatrix}, \quad \beta = \begin{pmatrix} 1 & 1 \\ 1 & 1 \end{pmatrix}, \quad \text{and} \quad \gamma = \begin{pmatrix} 1 & 1 \\ 1 & 1 \end{pmatrix}.$$

We consider aggregations over both time and space for both processes. For ease of visualization, we aggregate data using the same coarseness for time and space, and separately for each process, i.e  $\Delta_1^t = \Delta_1^\kappa = \Delta_1$  and  $\Delta_2^t = \Delta_2^\kappa = \Delta_2$ , where the subscript is used to indicate process 1 and 2. This is not necessary, and in our study of Section 5 we consider aggregations of different sizes. We consider 9 different data aggregations by varying  $\Delta_1$  and  $\Delta_2$  over the values 0, 0.75 and 1.

Applying our method on the aggregated data sets result in good estimates on average (Table A.4). The bias for the estimated parameters is consistently low over all aggregations we considered, ranging from -0.009 to 0.061 across all parameters and aggregations. Moreover, coverage varies from 92.3 to 97%. Similar to the univariate case, we see that the estimate of  $\mu$  and  $\alpha$  are very stable over different aggregations, with credible interval lengths that increase very slightly as the aggregations get coarser. Compared to these parameters,  $\beta$  and  $\gamma$  are more sensitive to coarser aggregations. Figure 5 shows the mean credible interval lengths for  $\beta$  and  $\gamma$  over different aggregation sizes. We find that the CI length for parameters that correspond to self-excitation ( $\beta_{11}, \beta_{22}, \gamma_{11}, \gamma_{22}$ ) are affected most by aggregation in the process they represent; coarser aggregation in process 1 leads to higher credible interval length for  $\beta_{11}, \gamma_{11}$  and little impact on the credible interval lengths for  $\beta_{22}, \gamma_{22}$ , while the reverse is true for coarser aggregation in process 2. In contrast, parameters which correspond to external-excitation ( $\beta_{12}, \beta_{21}, \gamma_{12}, \gamma_{21}$ ) are similarly affected by aggregation in either process.

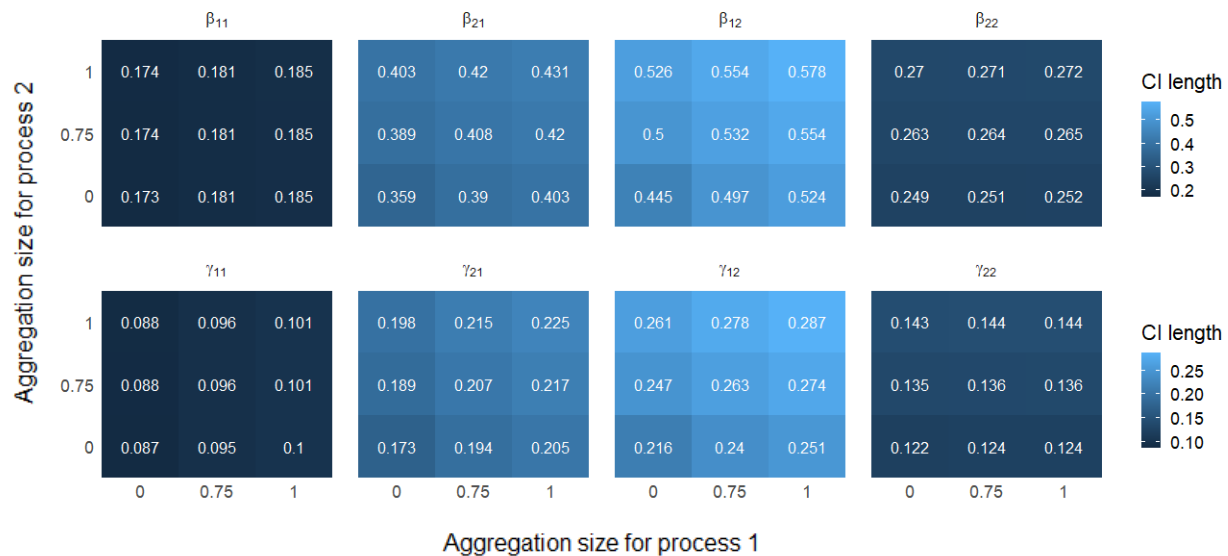


**Figure 5:** Average credible interval length for  $\beta_{m,l}$  and  $\gamma_{m,l}$  where  $m, l \in \{1, 2\}$  over 400 simulated multiple spatio-temporal data sets and based on different aggregation sizes in each process

## 5 Application

We illustrate our method using real data of insurgent violence incidents in Iraq. Our data record time, location (latitude and longitude) and type of insurgent violence events. We focus on small arms fire (SAF) and improvised explosive device (IED) attacks from October–December 2006. We study a relatively short time period during which we could assume that the process’ dynamics are relatively constant. During the time period under study, there are 4,335 SAF attacks and 4,526 IED attacks, and the events are recorded at the minute-level with spatial resolutions at the  $10^{-5}$  scale. We recognise that the available data might be subject to measurement error which we do not account for here. Instead, in the rare occasion that events are recorded to occur at exactly the same time or the same location, they are minimally jittered before any analysis by adding a draw from a uniform  $U(0, 1/120)$  (in hours) and a  $U(0, 5 \times 10^{-6})$  (in degrees) distribution to the recorded time, and recorded latitude and longitude entries, respectively. We consider the resulting event timestamps and locations as the exact data for this study, and we investigate the method’s performance under coarser aggregations. The two processes are expected to have self-exciting behaviors (Lewis and Mohler, 2011), and are potentially mutually exciting. We consider temporal (Section 5.1), spatio-temporal (Section 5.2), and mutually-exciting spatio-temporal (Section 5.3) models for analyzing their behavior.

### 5.1 Temporal analysis

In this section, we ignore the available spatial information and possible mutual excitement, and we fit the temporal model on SAF and IED attacks separately. We fit the model on the exact data and on aggregated data with aggregation size corresponding to  $1/60, 1/2, 1$  and  $3/2$  hours. We use a  $\text{Gamma}(1, 1)$  prior on  $\beta$  that assigns a low probability on very large values of  $\beta$  and small values of  $1/\beta$ , since we do not expect instantaneous excitement for attack events. The temporal model on the exact data for IED attacks returns a posterior mean of  $\beta$  that is equal to 0.93 indicating that it takes on average  $1/0.93 = 1.08$  hours for an IED attack to trigger another attack. Therefore, the one and a half hour aggregation we consider is relatively coarse with respect to the process’ temporal self-excitement period.

Figure 6 shows the posterior mean and 95% credible intervals of  $\mu, \alpha, \beta$  in the model fitted with exact data and aggregated data respectively, and separately for IED and SAF attacks. In both analyses, the

posterior mean for  $\mu$ ,  $\alpha$  and  $\beta$  are relatively stable across aggregation sizes. Similarly to what we observed in our simulations for aggregated temporal data (Section 4.1), the credible interval lengths for  $\mu$  and  $\alpha$  are almost unchanged for coarser temporal aggregations. In IED analysis, the length of the credible interval for  $\beta$  increases from 0.21 to 0.29, reflecting the uncertainty induced by the aggregation. The uncertainty in the estimate of  $\beta$  is less affected in the model for the SAF attacks compared to the IED attacks. One possible reason is that the estimated  $\alpha$  for SAF data is larger than that for IED data, implying that this dataset involves a higher offspring/immigrant ratio, in which case the estimation for  $\beta$  is more stable across aggregation sizes as we found in our simulations (Section 4.1).

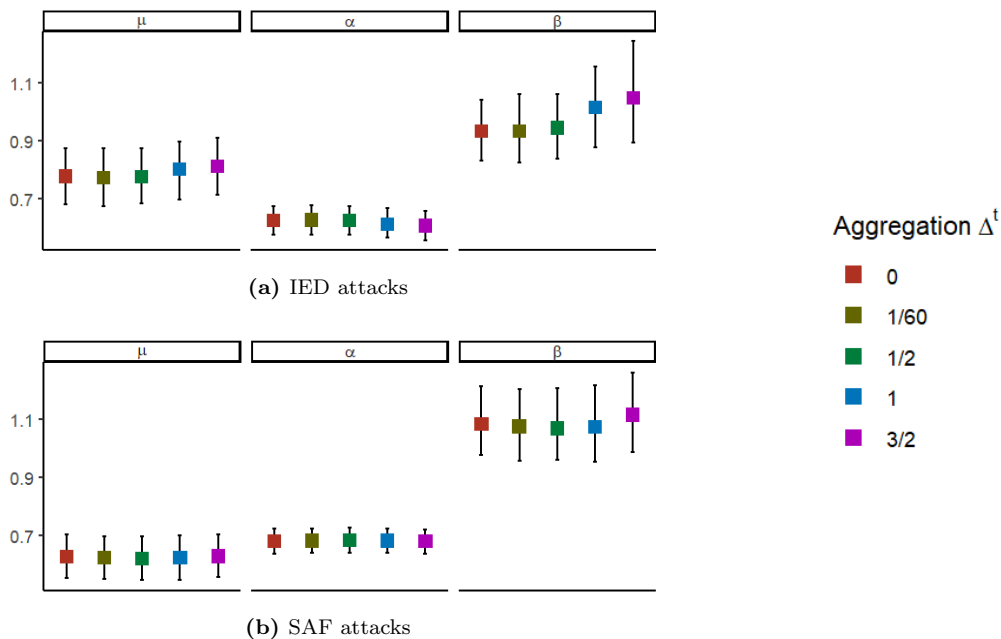


**Figure 6:** Posterior means and 95% credible intervals of parameters using the exact and aggregated data for IED and SAF attacks using a temporal model.

## 5.2 Spatio-temporal analysis

In this section, we extend the temporal analysis to include the events' spatial information by fitting the spatio-temporal model on the SAF and IED event data separately. Figure 7a shows the location of IED and SAF attacks during our study period. The location of the events are not evenly distributed around the country, but they are mostly concentrated around Baghdad, Mosul and Al Basrah, and most of them are very close to the road network. Thus, assuming a uniform distribution for the spatial marks of the immigrants

over the study area is not appropriate in this case. We modify the spatio-temporal model to specify that the location of the immigrants follows a mixture distribution:

$$\gamma_I(\kappa) = \frac{\rho}{2\pi\gamma_{c_1}\gamma_r} \exp\left\{-\frac{d_{c_1}^2(\kappa)}{2\gamma_{c_1}^2} - \frac{d_r^2(\kappa)}{2\gamma_r^2}\right\} + \frac{1-\rho}{2\pi\gamma_{c_2}\gamma_r} \exp\left\{-\frac{d_{c_2}^2(\kappa)}{2\gamma_{c_2}^2} - \frac{d_r^2(\kappa)}{2\gamma_r^2}\right\}, \quad (5)$$

where  $d_r(\kappa)$  is the closest distance of point  $\kappa$  from the road network,  $d_{c_1}(\kappa)$  is the distance of point  $\kappa$  from Baghdad, and  $d_{c_2}(\kappa)$  is the closest distance of point  $\kappa$  from Mosul and Al Basrah. One could consider a 3-way mixture distribution by allowing a separate distance from Mosul and Al Basrah. However, we find that the patterns of events near those two cities are similar, and therefore we consider them simultaneously. The parameter  $\rho \in (0,1)$  denotes the mixture parameter, specifying the relative prevalence of immigrants arising from the one versus the other distribution. Figure 7b shows the estimated immigrant mark density for the IED data, which matches the observed patterns of IED locations quite accurately.

The prior distributions for the additional variance parameters are specified to be independent conjugate priors:  $\gamma_r^2 \sim \text{IG}(0.001, 0.001)$ ,  $\gamma_{c_1}^2 \sim \text{IG}(0.001, 0.001)$ , and  $\gamma_{c_2}^2 \sim \text{IG}(0.001, 0.001)$ , and the prior for  $\rho$  is assumed to be  $\rho \sim \text{Beta}(1, 1)$ . Sampling steps for these additional parameters are added to the procedure described in Section 3.4. Specifically, for the events labels as immigrants at each step of the MCMC, we introduce a latent variable  $z \sim \text{Bernoulli}(\rho)$  conditional on which

$$\gamma_I(\kappa|z=1) = \frac{1}{2\pi\gamma_{c_1}\gamma_r} \exp\left\{-\frac{d_{c_1}^2(\kappa)}{2\gamma_{c_1}^2} - \frac{d_r^2(\kappa)}{2\gamma_r^2}\right\} \quad \text{and} \quad \gamma_I(\kappa|z=0) = \frac{1}{2\pi\gamma_{c_2}\gamma_r} \exp\left\{-\frac{d_{c_2}^2(\kappa)}{2\gamma_{c_2}^2} - \frac{d_r^2(\kappa)}{2\gamma_r^2}\right\}.$$

Note that we only need  $z$  for immigrants, and additional parameters are  $(\gamma_r, \gamma_{c_1}, \gamma_{c_2}, \mathbf{z})$ , where  $\mathbf{z} = \{z_i : i \in I\}$ . Then the conditional posteriors for these parameters are:

$$\begin{aligned} z_i | \mathbf{N}, \mathbf{x}, \mathbf{Y}, \theta, \rho &\sim \text{Bernoulli}\left(\frac{\rho\gamma_I(\kappa_i|z_i=1)}{\rho\gamma_I(\kappa_i|z_i=1) + (1-\rho)\gamma_I(\kappa_i|z_i=0)}\right) \\ \gamma_r^2 | \mathbf{N}, \mathbf{x}, \mathbf{Y}, \mathbf{z} &\sim \text{IG}\left(0.001 + |I|, 0.001 + \frac{1}{2} \sum_{i \in I} d_r^2(\kappa_i)\right) \\ \gamma_{c_1} | \mathbf{N}, \mathbf{x}, \mathbf{Y}, \mathbf{z} &\sim \text{IG}\left(0.001 + \sum_{i \in I} 1\{z_i=1\}, 0.001 + \frac{1}{2} \sum_{i \in I} d_{c_1}^2(\kappa_i)\right) \\ \gamma_{c_2} | \mathbf{N}, \mathbf{x}, \mathbf{Y}, \mathbf{z} &\sim \text{IG}\left(0.001 + \sum_{i \in I} 1\{z_i=0\}, 0.001 + \frac{1}{2} \sum_{i \in I} d_{c_2}^2(\kappa_i)\right), \quad \text{and} \end{aligned}$$

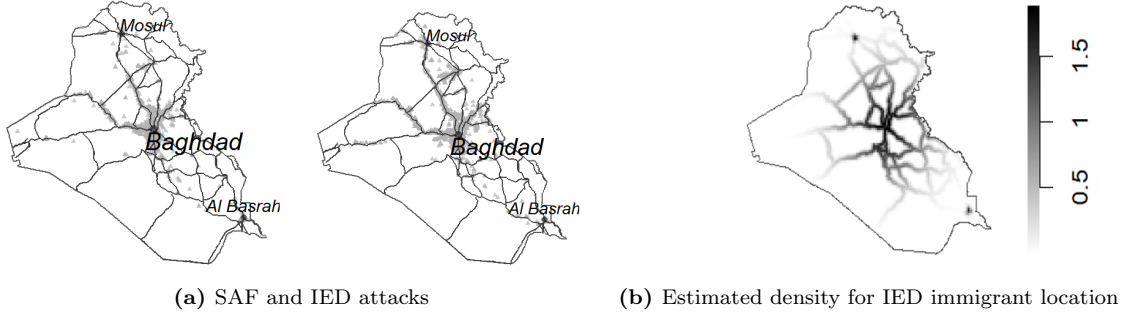


**Figure 7:** (a) Locations of SAF and IED attacks in Iraq from October-December 2006. Attacks are mostly concentrated near the three cities and the main road network. (b) Estimated immigrant mark density for exact IED data, where  $\gamma = 0.0046$ ,  $\gamma_r = 0.063$ ,  $\gamma_{c_1} = 1.31$ ,  $\gamma_{c_2} = 0.09$  and  $\rho = 0.94$ .

$$\rho | \mathbf{N}, \mathbf{x}, \mathbf{Y}, \mathbf{z} \sim \text{Beta}\left(1 + \sum_{i \in I} 1\{z_i = 1\}, 1 + \sum_{i \in I} 1\{z_i = 0\}\right).$$

We examine the performance of our method based on different coarseness of aggregation. Using the exact data, we find that the posterior mean of  $\beta$  is approximately 0.01 for both processes, meaning that it takes on average about 100 hours for an event to trigger another event when spatial information is incorporated. Therefore, we consider hourly and daily temporal aggregations, i.e.  $\Delta^t = 1, 24$  (hours), as these aggregations are commonly seen in practice. We also find that, based on the exact data, the estimates of the location parameters  $(\gamma, \gamma_r, \gamma_{c_1}, \gamma_{c_2})$  in the mark distribution are equal to  $(0.0054, 0.062, 1.04, 0.09)$  for SAF attacks and  $(0.0046, 0.063, 1.31, 0.087)$  for IED attacks. Approximately, 1 degree is equal to 111 kilometers, so these estimates correspond to about  $(0.6, 6.9, 115.4, 10)$  and  $(0.5, 7, 145, 9.7)$  kilometers, respectively. Based on the smallest value, we choose to aggregate the space with  $\Delta^\kappa \in \{0.001, 0.005\}$ , corresponding to a little over 100 meters, and 0.5 kilometer.

Figure 8 shows the posterior mean and 95% intervals of all parameters in the marked Hawkes process  $(\mu, \alpha, \beta, \gamma, \gamma_r, \gamma_{c_1}, \gamma_{c_2}, \rho)$  using exact and aggregated data for IED and SAF attacks separately. Focusing on the results for the SAF attacks in Figure 8b, we find that for a fixed value of  $\Delta^\kappa$ , results on all these parameters are comparable across temporal aggregations: the posterior means remain nearly the same and the credible interval length increases very little as  $\Delta^t$  increase. The impact of coarser spatial aggregations (larger values of  $\Delta^\kappa$ ) on estimated parameters is more prevalent. We focus first on the posterior distribution for the parameters in the distribution of the immigrant marks  $(\gamma_r, \gamma_{c_1}, \gamma_{c_2}, \rho)$ . We find that the posterior

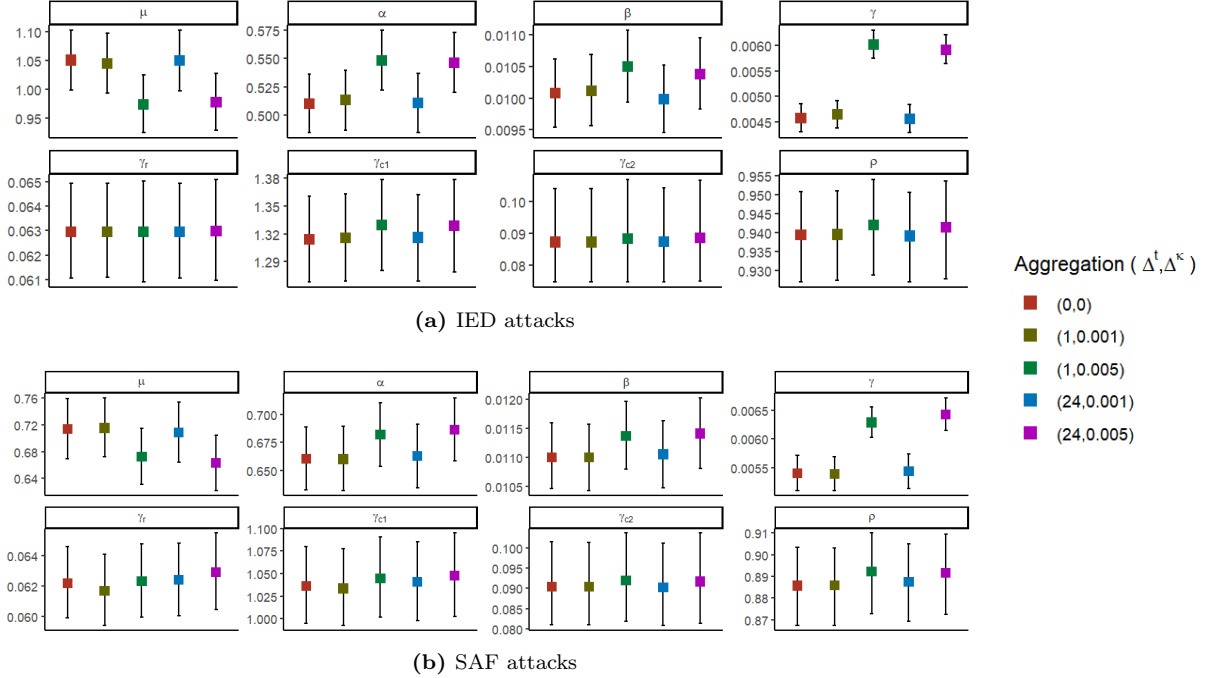


**Figure 8:** Posterior means and 95% credible intervals of parameters using exact and aggregated spatio-temporal data.

mean for these parameters is similar across spatial aggregations. The corresponding credible interval lengths increase slightly for larger values of  $\Delta^\kappa$ , with percentage change in the credible interval length ranging from 2.31% to 8.82% for the coarsest aggregation size considered. When investigating the posterior distribution of  $\mu$ ,  $\alpha$ ,  $\beta$ , and  $\gamma$ , we find that the posterior mean changes significantly for the coarsest spatial aggregation ( $\Delta^\kappa = 0.005$ .) Possible reasons are that the number of events in some space grid is large and we may not have enough information to learn the true parameters, or that the multivariate normal distribution may not accurately capture the distribution of the offspring marks given the fact that many events occurs at nearly the same place. We do the same analysis on the IED data and get comparable result shown in Figure 8a.

### 5.3 Mutually exciting process analysis

Finally, we model IED and SAF data allowing for mutual excitement. We consider aggregated SAF and IED data using the same aggregation size in time and space as in Section 5.2, i.e.  $\Delta_1^t = \Delta_2^t \in \{1, 24\}$  and  $\Delta_1^\kappa = \Delta_2^\kappa \in \{0.001, 0.005\}$ . We maintain the distribution of immigrant locations in (5), and we specify the same priors for the additional, cross-excitement parameters. Figure 9 shows the posterior mean

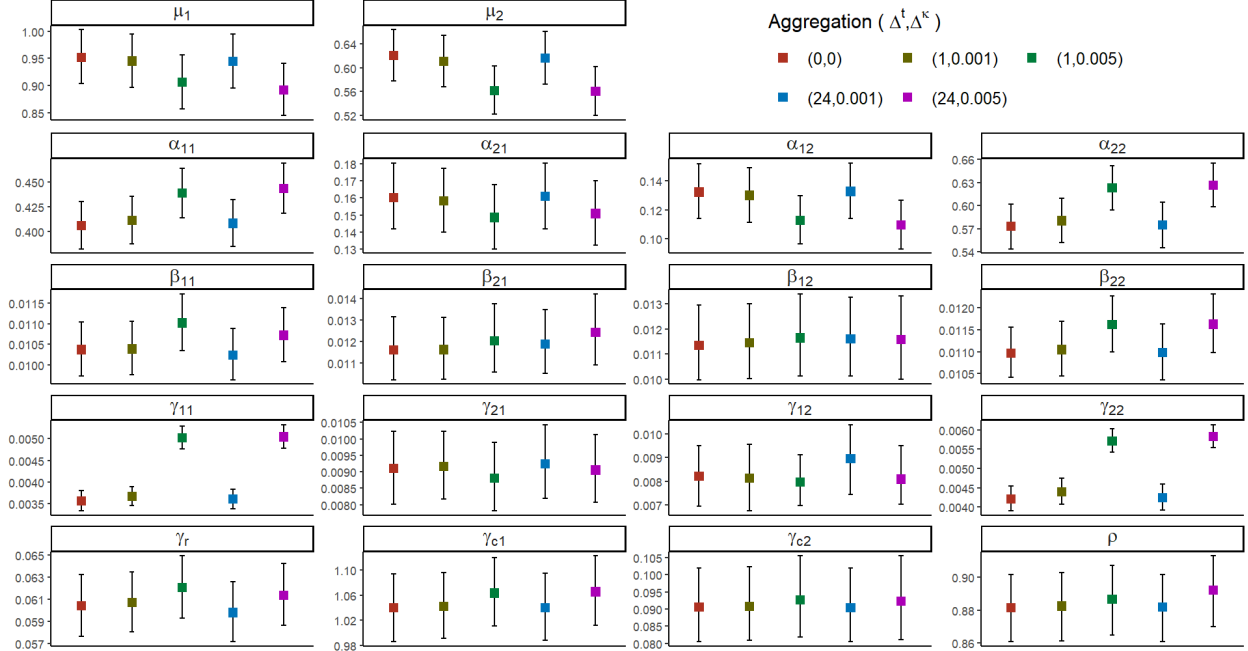


**Figure 9:** Posterior means and 95% credible intervals of parameters from the mutually-exciting Hawkes process using exact and aggregated spatio-temporal data. Process 1: IED, process 2: SAF.

and 95% for all parameters over different aggregation. We note that estimates of  $\mu$  and  $\alpha$  for the self-excitation ( $\mu_1, \mu_2, \alpha_{11}, \alpha_{22}$ ) are smaller than corresponding estimates in Section 5.2. This occurs because some events that were previously labeled as immigrants or offsprings due to self-excitation are now labeled offsprings due to external-excitation. Moreover, the effects of aggregation on those parameters are similar to that on corresponding parameters in Section 5.2. For example, we can see the changes in  $\beta_{22}$  estimate is comparable to  $\beta$  estimate shown in Figure 8b. For  $\beta$  and  $\gamma$ , the posterior means of external-excitation parameters ( $\beta_{12}, \beta_{21}, \gamma_{12}, \gamma_{21}$ ) are more sensitive to the aggregation in space compare to self-excitation parameters ( $\beta_{11}, \beta_{22}, \gamma_{11}, \gamma_{22}$ ). More specifically, the credible interval lengths of  $\beta_{12}$  and  $\beta_{21}$  range from 0.0011 to 0.0014, and the credible interval lengths of  $\beta_{11}$  and  $\beta_{22}$  range from 0.0029 to 0.0033 across all aggregation considered.

## 6 Discussion

In this paper, we proposed a Bayesian estimation procedure for aggregated Hawkes processes. We handle the aggregation by treating the exact data as latent variables updated by an extra step in the MCMC algorithm



for exact Hawkes processes. We examine the effect of aggregation sizes in time and space in different scenarios. Compared with a frequentist method for aggregated temporal Hawkes processes (Shlomovich *et al.*, 2022), our method achieves comparable or lower bias on simulated data, and provides a straightforward way to perform inference and incorporate spatial information. Our method is applicable for temporal and spatio-temporal point pattern data, as well as data on multiple processes. We analyze real data on insurgent violence attacks in Iraq and find consistent results across different aggregation sizes.

One issue that is ignored in this paper is the edge effects in both time and space. We assume that no events happened before  $t = 0$ , which does not hold in practice. Moreover, offsprings of events near the boundary might occur outside the observed temporal window and, as a result, are not included in our data, which can affect parameter estimates. Some edge correction methods are discussed in Lapham (2014), Diggle (2013) and Cronie and Särkkä (2011). Implementing edge correction in our framework can be explored in future work.

Additional work on aggregated point pattern data can extend in various directions. Firstly, our method could be extended to incorporate aggregation of marks other than spatial coordinates, or multivariate marks where aggregation of mark information might blur our ability to learn their correlation structure. Secondly, it would be interesting to investigate nonparametric Hawkes process models in the presence of aggregated point pattern data, which are used in many applications for extra flexibility. For instance, Lewis and Mohler (2011), Fox *et al.* (2016) and Marsan and Lengline (2008) introduce ways to incorporate nonparametric inhomogeneous  $\mu(t)$ , and Zhou *et al.* (2013) and Kirchner and Bercher (2018) use kernel density estimation for the offspring intensity. Moreover, the multivariate Hawkes process has been extended to allow for inhibition effects within a Bayesian estimation procedure (Deutsch and Ross, 2022), which can be explored within the realm of aggregated data as well. Lastly, it is of interest to us to investigate the implications of using aggregated point pattern data for learning causal dependencies among processes (Papadogeorgou *et al.*, 2020), especially when these effects might manifest almost instantaneously in time.

## References

- Aldor-Noiman, S., Brown, L. D., Fox, E. B., and Stine, R. A. (2016). Spatio-temporal low count processes with application to violent crime events. *Statistica Sinica* 1587–1610.
- Bu, F., Aiello, A. E., Xu, J., and Volfovsky, A. (2022). Likelihood-based inference for partially observed epidemics on dynamic networks. *Journal of the American Statistical Association* **117**, 537, 510–526.
- Chiang, W.-H., Liu, X., and Mohler, G. (2022). Hawkes process modeling of covid-19 with mobility leading indicators and spatial covariates. *International journal of forecasting* **38**, 2, 505–520.
- Cronie, O. and Särkkä, A. (2011). Some edge correction methods for marked spatio-temporal point process models. *Computational Statistics and Data Analysis* **55**, 7, 2209–2220.
- Darolles, S., Le Fol, G., Lu, Y., and Sun, R. (2019). Bivariate integer-autoregressive process with an application to mutual fund flows. *Journal of Multivariate Analysis* **173**, 181–203.
- Daryl, D. and Vere-Jones, D. (2003). *An introduction to the theory of point processes: volume I: elementary theory and methods*. Springer.
- Deutsch, I. and Ross, G. J. (2022). Bayesian estimation of multivariate hawkes processes with inhibition and sparsity. *arXiv preprint arXiv:2201.05009* .
- Diggle, P. J. (2013). *Statistical analysis of spatial and spatio-temporal point patterns*. CRC press.
- Fox, E. W., Schoenberg, F. P., and Gordon, J. S. (2016). Spatially inhomogeneous background rate estimators and uncertainty quantification for nonparametric hawkes point process models of earthquake occurrences. *The Annals of Applied Statistics* **10**, 3, 1725–1756.
- Hawkes, A. G. (1971). Spectra of some self-exciting and mutually exciting point processes. *Biometrika* **58**, 1, 83–90.
- Hawkes, A. G. and Oakes, D. (1974). A cluster process representation of a self-exciting process. *Journal of Applied Probability* **11**, 3, 493–503.

- Kirchner, M. (2016). Hawkes and INAR ( $\infty$ ) processes. *Stochastic Processes and their Applications* **126**, 8, 2494–2525.
- Kirchner, M. (2017). An estimation procedure for the hawkes process. *Quantitative Finance* **17**, 4, 571–595.
- Kirchner, M. and Bercher, A. (2018). A nonparametric estimation procedure for the hawkes process: comparison with maximum likelihood estimation. *Journal of Statistical Computation and Simulation* **88**, 6, 1106–1116.
- Lapham, B. M. (2014). *Hawkes processes and some financial applications*. Master’s thesis, University of Cape Town.
- Lewis, E. and Mohler, G. (2011). A nonparametric em algorithm for multiscale hawkes processes. *Journal of Nonparametric Statistics* **1**, 1, 1–20.
- Lewis, E., Mohler, G., Brantingham, P. J., and Bertozzi, A. L. (2012). Self-exciting point process models of civilian deaths in iraq. *Security Journal* **25**, 3, 244–264.
- Marsan, D. and Lengline, O. (2008). Extending earthquakes’ reach through cascading. *Science* **319**, 5866, 1076–1079.
- Ogata, Y. (1998). Space-time point-process models for earthquake occurrences. *Annals of the Institute of Statistical Mathematics* **50**, 2, 379–402.
- Papadogeorgou, G., Imai, K., Lyall, J., and Li, F. (2020). Causal inference with spatio-temporal data: estimating the effects of airstrikes on insurgent violence in iraq. *arXiv preprint arXiv:2003.13555* .
- Porter, M. D. and White, G. (2012). Self-exciting hurdle models for terrorist activity. *The Annals of Applied Statistics* **6**, 1, 106–124.
- Rasmussen, J. G. (2013). Bayesian Inference for Hawkes Processes. *Methodology and Computing in Applied Probability* **15**, 623–642.
- Shlomovich, L., Cohen, E. A., and Adams, N. (2021). A parameter estimation method for multivariate aggregated hawkes processes. *arXiv preprint arXiv:2108.12357* .

- Shlomovich, L., Cohen, E. A., Adams, N., and Patel, L. (2022). Parameter estimation of binned Hawkes processes. *Journal of Computational and Graphical Statistics* 1–11.
- Tucker, J. D., Shand, L., and Lewis, J. R. (2019). Handling missing data in self-exciting point process models. *Spatial statistics* **29**, 160–176.
- Veen, A. and Schoenberg, F. P. (2008). Estimation of space–time branching process models in seismology using an em–type algorithm. *Journal of the American Statistical Association* **103**, 482, 614–624.
- Zhou, K., Zha, H., and Song, L. (2013). Learning triggering kernels for multi-dimensional Hawkes processes. In *International conference on machine learning*, 1301–1309. PMLR.

# SUPPLEMENTARY APPENDIX FOR “BAYESIAN INFERENCE FOR AGGREGATED HAWKES PROCESSES”

## Table of Contents

<b>A</b>	<b>Table of notation</b>	<b>2</b>
<b>B</b>	<b>Multiple Hawkes processes</b>	<b>2</b>
B.1	Latent variable formulation . . . . .	2
B.2	Estimation and inference within the Bayesian framework . . . . .	2
<b>C</b>	<b>Additional simulation results</b>	<b>4</b>
C.1	Simulation results for temporal data . . . . .	4
C.2	Simulation results for spatio-temporal data. . . . .	4
C.3	Simulation results for multiple spatial temporal data . . . . .	4

## A Table of notation

Table A.1: Notation

$X = \{(t_i, \kappa_i)\}$	A marked process
$\theta$	Parameter vector for marked Hawkes process
$\mathbf{Y}$	Branching structure
$I$	Collection of all immigrants
$O$	Collection of all offspring
$O_j$	Collection of all offspring of events $j$
$\mu(t)$	Background intensity
$\alpha(\kappa)$	Total offspring intensity
$\beta(t, \kappa)$	Normalized offspring intensity
$\gamma_I(\kappa)$	Immigrant mark density
$\gamma_{O_j}(\kappa (t_j, \kappa_j))$	offspring mark density for events in $O_j$
$\Delta^t$	Aggregation size in time
$\Delta^\kappa$	Aggregation size in space
$B_i^t$	$i^{\text{th}}$ Time bins
$B_i^\kappa$	$i^{\text{th}}$ Space bins
$N_{i,j}$	Number of events in $B_i^t \times B_j^\kappa$

## B Multiple Hawkes processes

### B.1 Latent variable formulation

Suppose we observe  $L$  aggregated Hawkes processes on  $[0, T] \times W$ . Assuming the same notations in Section 3.1, the observed data is  $\mathbf{N} = \{N_{l,i,j} : l = 1, \dots, L, i = 1, \dots, n_{l,1}, j = 1, \dots, n_{l,2}\}$ . Let  $x = \{(t_{l,i}, \kappa_{l,i}) : l = 1, \dots, L, i = 1, \dots, n_l\}$  be the underlying exact data which is unobserved, and  $\mathbf{Y} = \{Y_{l,i} : l = 1, \dots, L, i = 1, \dots, n_l\}$  be the latent branching structure. The parameters for the continuous Hawkes process are now  $\theta = (\mu, \alpha, \beta, \gamma)$ , where  $\mu = (\mu_l : l = 1, \dots, L)$ ,  $\alpha = (\alpha_{m,l} : m, l = 1, \dots, L)$ ,  $\beta = (\beta_{m,l} : m, l = 1, \dots, L)$ ,  $\gamma = (\gamma_{m,l} : m, l = 1, \dots, L)$ . In this case, the distribution of aggregated data  $p(\mathbf{N}|\mathbf{x}, \mathbf{Y}, \theta)$  is equal to 1 only when the aggregated data agrees the exact data for each process:  $\sum_{i=1}^{n_1} \sum_{j=1}^{n_2} N_{i,j} = n_l$  and  $\sum_{k=1}^{n_l} 1\{(t_{l,k}, \kappa_{l,k}) \in B_{l,i}^t \times B_{l,j}^\kappa\} = N_{l,i,j}$  for all  $i, j, l$ . Similar to Section 3.2, we need to sample from  $p(\mathbf{x}|\mathbf{Y}, \theta)$  and  $p(\theta, \mathbf{Y}|\mathbf{x})$  iteratively.

### B.2 Estimation and inference within the Bayesian framework

For  $m, l \in \{1, \dots, L\}$ , we assume (independent) gamma priors for  $\mu_l$ ,  $\alpha_{m,l}$  and  $\beta_{m,l}$ , and inverse gamma priors for  $\gamma_{m,l}^2$ :

$$\mu_l \sim \text{Gamma}(a_{l,1}, b_{l,1}), \alpha_{m,l} \sim \text{Gamma}(a_{m,l,2}, b_{m,l,2}), \beta_{m,l} \sim \text{Gamma}(a_{m,l,3}, b_{m,l,3}), \gamma_{m,l}^2 \sim \text{IG}(a_{m,l,4}, b_{m,l,4}).$$

For  $i = 1, 2, \dots, n_l$ , we assume a discrete uniform distribution on feasible values of  $Y_{l,i}$ , i.e.  $Y_{l,i} \sim \text{Unif}(\{(0, 0)\} \cup \{(k, j) : t_{k,j} < t_{l,i}\})$ . Given the latent branching structure and model parameters, the distribution of exact data (under the model specification in Section 3.3) is

$$\begin{aligned} p(\mathbf{x}|\mathbf{Y}, \theta) &= \prod_{l=1}^L \exp(-\mu_l T) (\mu_l |W|^{-1})^{|I_l|} \\ &\times \prod_{m=1}^L \prod_{i=1}^{n_m} \prod_{l=1}^L \left\{ \exp \left\{ -\alpha_{m,l} \{1 - \exp[-\beta_{m,l}(T - t_{m,i})]\} \right\} \right. \\ &\times \left. \prod_{t_{l,j} \in O_{m,i}} \frac{\alpha_{m,l} \beta_{m,l}}{\sqrt{2\pi} \gamma_{m,l}^2} \exp \left[ -\beta_{m,l}(t_{l,j} - t_{m,i}) - \frac{\|\kappa_{l,j} - \kappa_{m,i}\|^2}{2\gamma_{m,l}^2} \right] \right\}, \end{aligned}$$

where  $I_l$  denotes the set of immigrants in process  $l$  and  $O_{m,i}$  denotes the set of offsprings of event  $i$  in process  $m$ .

We use Gibbs sampling for each of the parameter in  $\theta$  and the latent branching structure  $\mathbf{Y}$ . Specifically, we iteratively sample from

$$\begin{aligned} \mu_l | \mathbf{x}, \theta_{-\mu_l}, \mathbf{Y}, \mathbf{N} &\sim \text{Gamma}(a_{l,1} + |I_l|, b_{l,1} + T) \\ \alpha_{m,l} | \mathbf{x}, \theta_{-\alpha_{m,l}}, \mathbf{Y}, \mathbf{N} &\sim \text{Gamma}(a_{m,l,2} + \sum_{i=1}^{n_m} |O_{m,i}|, b_{m,l,2} + \sum_{i=1}^{n_m} \beta_{m,l} \exp(-\beta_{m,l}(T - t_{m,i}))) \\ \gamma_{m,l}^2 | \mathbf{x}, \theta_{-\gamma_{m,l}}, \mathbf{Y}, \mathbf{N} &\sim \text{IG}(a_{m,l,4} + \sum_{i=1}^{n_m} |O_{m,i}|, b_{m,l,4} + \frac{1}{2} \sum_{i=1}^{n_m} \sum_{t_{l,j} \in O_{m,i}} \|\kappa_{l,j} - \kappa_{m,i}\|^2), \end{aligned}$$

The full conditional of  $Y_{l,i}$  is a multinomial distribution given by

$$P(Y_{l,i} = (m, j) | \theta, \mathbf{Y}) \propto \begin{cases} \mu_l |W|^{-1}, & \text{for } m = j = 0, \text{ and} \\ \frac{\alpha_{m,l} \beta_{m,l}}{\sqrt{2\pi} \gamma_{m,l}^2} \exp(-\beta_{m,l}(t_{l,i} - t_{m,j}) - \frac{\|\kappa_{l,i} - \kappa_{m,j}\|^2}{2\gamma_{m,l}^2}), & \text{for } m > 0, j > 0, t_{m,k} < t_{l,i} \end{cases}$$

Let  $\mathbf{t}, \boldsymbol{\kappa}$  denote vectors of the exact time and spatial marks of all events respectively. Since there are no conjugate priors for  $\mathbf{t}, \boldsymbol{\kappa}$  and  $\beta_{m,l}$ . We use element-wise Metropolis-Hasting to sample from their full conditionals. Specifically, we propose value  $\beta'_{m,l}$  from a normal distribution with mean  $\beta^c_{m,l}$  and standard deviation  $\sigma_{\beta_{m,l}}$ . We accept the move with probability

$$\begin{aligned} H_{\beta_{m,l}} &= \min \left( 1, \left( \frac{\beta'_{m,l}}{\beta^c_{m,l}} \right)^{a_{m,l,3}-1} \exp(b_{m,l,3}(\beta^c_{m,l} - \beta'_{m,l})) \right. \\ &\quad \prod_{i=1}^{n_m} \left\{ \exp \left( \alpha_{m,l} \exp(-\beta'_{m,l}(T - t_{m,i})) - \alpha_{m,l} \exp(-\beta^c_{m,l}(T - t_{m,i})) \right) \right. \\ &\quad \times \left. \left. \prod_{j \in O_{m,i}} \frac{\beta'_{m,l}}{\beta^c_{m,l}} \exp \left( -(\beta'_{m,l} - \beta^c_{m,l})(t_{l,j} - t_{m,i}) \right) \right\} \right) \end{aligned}$$

For  $i = 1, 2, \dots, n_m$ ,  $t'_{m,i}$  is drawn from a continuous uniform distribution that satisfies the following restrictions:  $t'_{m,i}$  is within the time bin of event  $i$  in process  $m$ , it occurs after its parent event (if it has one,

$Y_{m,i} \neq (0,0)$ ), and before its offsprings (if any). The proposed value of  $t_{m,i}$  is accepted with probability

$$H_{t_{m,i}} = \min \left( 1, \exp \left( \alpha_{m,l} \beta_{m,l} \exp(-\beta_{m,l}(T - t_{m,i}^c)) - \alpha_{m,l} \beta_{m,l} \exp(-\beta_{m,l}(T - t'_{m,i})) \right) \right. \\ \left. - (|O_{m,i}| + 1 \{Y_{m,i} \neq (0,0)\}) \beta_{m,l} (t'_{m,i} - t_{m,i}^c) \right).$$

Similarly,  $\kappa_{m,i}$  is drawn from a uniform distribution on the space bin containing  $\kappa_{m,i}$  and the proposed move is accepted with probability

$$H_{\kappa_{m,i}} = \min \left( 1, \exp \left( \frac{-\|\kappa'_{m,i} - \kappa_{\text{pa}}\|^2 + \|\kappa_{m,i}^c - \kappa_{\text{pa}}\|^2}{2\gamma_{q,l}^2} 1\{Y_{m,i} \neq (0,0)\} + \sum_{j \in O_{m,i}} \frac{-\|\kappa'_{m,i} - \kappa_{l,j}\|^2 + \|\kappa_{m,i}^c - \kappa_{l,j}\|^2}{2\gamma_{m,l}^2} \right) \right),$$

where  $q$  is the process that contains the parent of  $t_{m,i}$ .

## C Additional simulation results

### C.1 Simulation results for temporal data

In Figure A.1, we show the boxplot of estimates when apply our method and MC-EM method for on 400 data sets generated by parameter set 2. These results compliment the results and text shown in Section 4.1 of the manuscript.

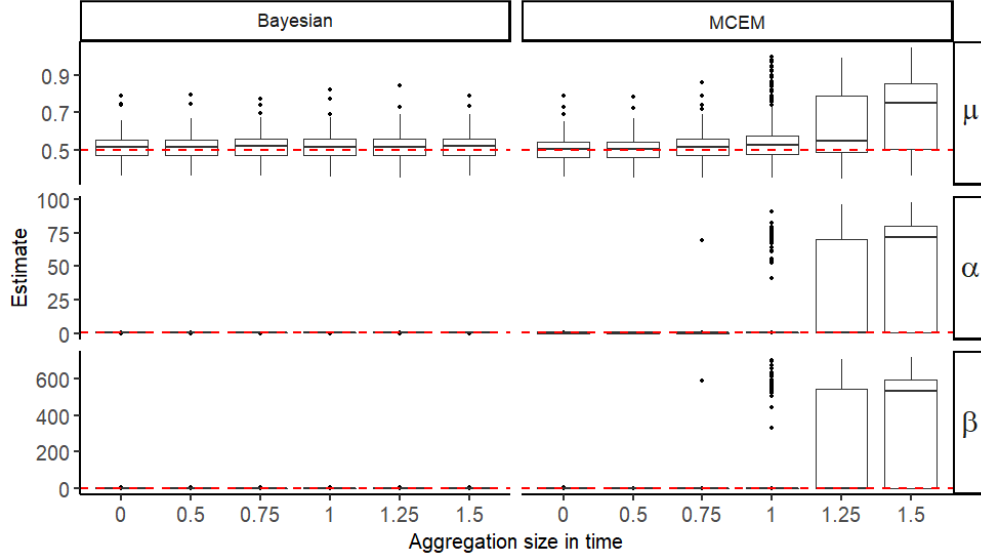
### C.2 Simulation results for spatio-temporal data.

In Table A.2 and Table A.3 we show the full spatio-temporal simulation results for parameter set 1 and parameter set 2, respectively. These results compliment the results and text shown in Section 4.2 of the manuscript.

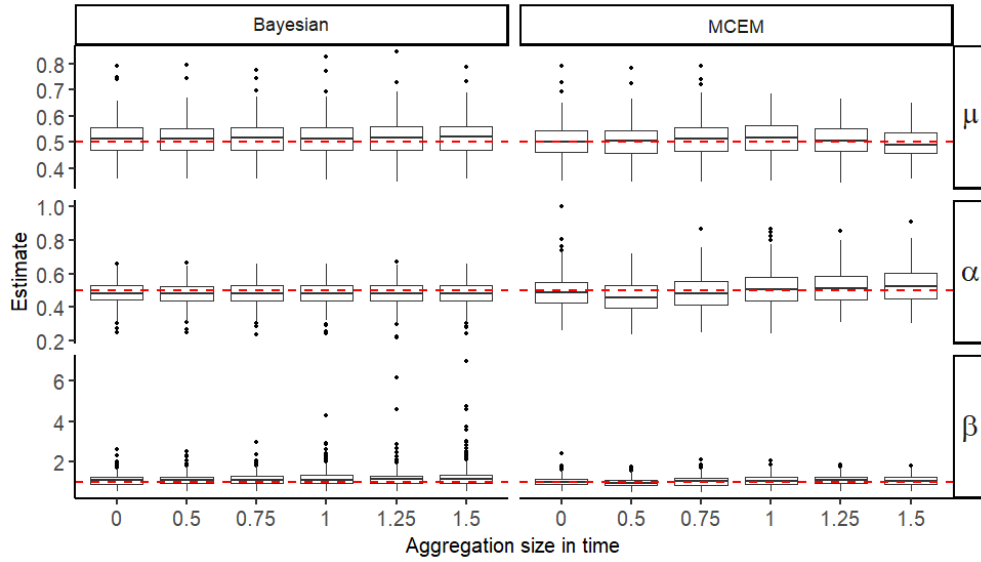
### C.3 Simulation results for multiple spatial temporal data

In Table A.4 we show the results of selected parameters for multiple spatio-temporal data. These results compliment the results and text shown in Section 4.3 of the manuscript.





(a) Include problematic estimates in MC-EM



(b) Remove problematic estimates in MC-EM

**Figure A.1:** Boxplot for estimates of  $\mu, \alpha$  and  $\beta$  using our Bayesian approach (left) and the MC-EM approach. The horizontal red lines indicate the true values which corresponding to parameter set 2:  $(\mu, \alpha, \beta) = (0.5, 0.5, 1)$

**Table A.2:** The result of the spatio-temporal simulation. The table shows the average posterior mean (“Estimate”), average 95% credible interval length (“CI length”), and coverage rate of the 95% credible interval (“Coverage”) for parameters  $\mu, \alpha$  and  $\beta, \gamma$  of the Hawkes process, across 400 simulated data sets. Parameter set:  $(\mu, \alpha, \beta, \gamma) = (0.3, 0.7, 1, 1)$

$\mu$					$\alpha$					
$\Delta^t$	$\Delta^\kappa$	Estimate	CI length	Coverage	$\Delta^t$	$\Delta^\kappa$	Estimate	CI length	Coverage	
0	0	0.3029	0.0969	0.95	0	0	0.6885	0.1491	0.9475	
	0.5	0.3029	0.0969	0.95		0.5	0.6885	0.149	0.95	
	1	0.3029	0.0969	0.9475		1	0.6885	0.1491	0.9525	
	1.5	0.3031	0.097	0.9525		1.5	0.6884	0.1491	0.95	
0.5	0	0.303	0.0969	0.9475	0.5	0	0.6885	0.1491	0.95	
	0.5	0.3029	0.0969	0.95		0.5	0.6885	0.1491	0.95	
	1	0.303	0.097	0.945		1	0.6884	0.1491	0.9525	
1	1.5	0.3031	0.0971	0.9475	1.5	1.5	0.6883	0.1492	0.9525	
	0	0.303	0.0969	0.95		1	0	0.6884	0.1491	0.95
	0.5	0.303	0.097	0.95			0.5	0.6884	0.1491	0.95
1	0.303	0.097	0.9475	1	0.6884		0.1492	0.9525		
1.5	1.5	0.3032	0.0971	0.9475	1.5	1.5	0.6882	0.1492	0.955	
	0	0.3026	0.0969	0.9574		1.5	0	0.6888	0.1491	0.9521
	0.5	0.3026	0.0969	0.9529			0.5	0.6886	0.1491	0.9581
	1	0.3027	0.097	0.9555			1	0.6886	0.1492	0.9581
1.5	0.3029	0.0971	0.9582	1.5	0.6884		0.1492	0.9608		

$\beta$					$\gamma$				
$\Delta^t$	$\Delta^\kappa$	Estimate	CI length	Coverage	$\Delta^t$	$\Delta^\kappa$	Estimate	CI length	Coverage
0	0	1.0204	0.2588	0.9475	0	0	0.9976	0.1296	0.9375
	0.5	1.0208	0.2597	0.95		0.5	0.9963	0.1336	0.9375
	1	1.0212	0.2613	0.9475		1	0.994	0.1447	0.9425
	1.5	1.0221	0.264	0.9375		1.5	0.9918	0.1605	0.94
0.5	0	1.0212	0.2629	0.955	0.5	0	0.9975	0.1314	0.93
	0.5	1.0217	0.2635	0.955		0.5	0.9962	0.1351	0.945
	1	1.0221	0.2648	0.955		1	0.994	0.1461	0.9325
	1.5	1.0229	0.2673	0.9425		1.5	0.992	0.1615	0.9375
1	0	1.0246	0.2723	0.94	1	0	0.9976	0.133	0.9375
	0.5	1.025	0.2728	0.94		0.5	0.9964	0.1367	0.94
	1	1.0252	0.2745	0.9425		1	0.9943	0.1473	0.925
	1.5	1.0266	0.2767	0.9325		1.5	0.9923	0.1625	0.935
1.5	0	1.0285	0.2842	0.9574	1.5	0	0.9973	0.1342	0.9309
	0.5	1.0276	0.2843	0.9634		0.5	0.9962	0.1379	0.9372
	1	1.0279	0.2856	0.9581		1	0.994	0.1483	0.9346
	1.5	1.0295	0.2884	0.9504		1.5	0.9921	0.1636	0.9295

**Table A.3:** Simulation results for spatio-temporal data. The table shows the average posterior mean (“Estimate”), average 95% credible interval length (“CI length”), and coverage rate of the 95% credible interval (“Coverage”) for parameters  $\mu, \alpha$  and  $\beta, \gamma$  of the Hawkes process, across 400 simulated data sets. Parameter set:  $(\mu, \alpha, \beta, \gamma) = (0.5, 0.5, 1, 1)$

$\mu$					$\alpha$					
$\Delta^t$	$\Delta^\kappa$	Estimate	CI length	Coverage	$\Delta^t$	$\Delta^\kappa$	Estimate	CI length	Coverage	
0	0	0.5029	0.125	0.95	0	0	0.4943	0.125	0.9425	
	0.5	0.503	0.125	0.9475		0.5	0.4942	0.1251	0.9425	
	1	0.503	0.1251	0.9475		1	0.4942	0.1251	0.945	
	1.5	0.5032	0.1252	0.95		1.5	0.494	0.1252	0.9425	
0.5	0	0.5029	0.125	0.95	0.5	0	0.4943	0.1251	0.9425	
	0.5	0.5029	0.125	0.945		0.5	0.4943	0.1251	0.94	
	1	0.503	0.1251	0.945		1	0.4942	0.1252	0.945	
1	1.5	0.5032	0.1252	0.95	1.5	1.5	0.494	0.1252	0.9425	
	0	0.5029	0.125	0.9475		0	0	0.4943	0.1252	0.9425
	0.5	0.503	0.1251	0.945			0.5	0.4942	0.1251	0.94
1	0.503	0.1251	0.945	1	0.4941		0.1252	0.945		
1.5	1.5	0.5033	0.1252	0.9475	1.5	1.5	0.4939	0.1253	0.9425	
	0	0.503	0.1251	0.9475		0	0	0.4942	0.1252	0.945
	0.5	0.5031	0.1251	0.9525			0.5	0.4941	0.1251	0.9425
1	0.5031	0.1252	0.9525	1	0.4941		0.1252	0.9425		
1.5	1.5	0.5033	0.1253	0.95	1.5	1.5	0.4939	0.1253	0.94	

$\beta$					$\gamma$					
$\Delta^t$	$\Delta^\kappa$	Estimate	CI length	Coverage	$\Delta^t$	$\Delta^\kappa$	Estimate	CI length	Coverage	
0	0	1.0226	0.2888	0.955	0	0	0.9947	0.145	0.945	
	0.5	1.0229	0.2892	0.9525		0.5	0.9936	0.15	0.9575	
	1	1.0235	0.2911	0.95		1	0.9919	0.1645	0.9425	
	1.5	1.0235	0.2932	0.9575		1.5	0.9867	0.1851	0.9475	
0.5	0	1.0229	0.2935	0.955	0.5	0	0.9946	0.1463	0.95	
	0.5	1.0231	0.2943	0.9575		0.5	0.9934	0.1513	0.9625	
	1	1.0237	0.2959	0.955		1	0.9915	0.1654	0.9425	
1	1.5	1.0239	0.2982	0.965	1.5	1.5	0.9865	0.186	0.95	
	0	1.0242	0.3052	0.945		0	0	0.9945	0.1478	0.9425
	0.5	1.0244	0.3058	0.9525			0.5	0.9933	0.1527	0.9625
1	1.0251	0.3076	0.9475	1	0.9916		0.1667	0.9475		
1.5	1.5	1.0255	0.3099	0.945	1.5	1.5	0.9862	0.1872	0.9525	
	0	1.0301	0.3231	0.9525		0	0	0.9948	0.149	0.95
	0.5	1.0305	0.3241	0.96			0.5	0.9936	0.1538	0.96
1	1.0314	0.3258	0.9475	1	0.9916		0.1677	0.955		
1.5	1.5	1.0317	0.3284	0.96	1.5	1.5	0.9865	0.1882	0.95	

**Table A.4:** The result of selected parameters  $(\mu_1, \alpha_{21}, \beta_{11}, \gamma_{21})$  in the multiple spatio-temporal simulation. True parameter:  $(\mu_1, \alpha_{21}, \beta_{11}, \gamma_{21}) = (0.3, 0.3, 1, 1)$

$\mu_1$					$\alpha_{21}$				
$\Delta_1$	$\Delta_2$	Estimate	CI length	Coverage	$\Delta_1$	$\Delta_2$	Estimate	CI length	Coverage
	0	0.3044	0.0983	0.9425		0	0.2994	0.089	0.9475
0	0.75	0.3046	0.0998	0.9475	0	0.75	0.2993	0.0912	0.9475
	1	0.3047	0.1003	0.9525		1	0.2992	0.0921	0.96
	0	0.3047	0.0999	0.9375		0	0.2994	0.0916	0.94
0.75	0.75	0.3048	0.1006	0.95	0.75	0.75	0.2993	0.0929	0.9525
	1	0.3047	0.101	0.9475		1	0.2994	0.0938	0.965
	0	0.3051	0.1004	0.94		0	0.2991	0.0927	0.9525
1	0.75	0.305	0.1011	0.945	1	0.75	0.2993	0.0939	0.95
	1	0.3053	0.1014	0.9575		1	0.2989	0.0947	0.96

$\beta_{11}$					$\gamma_{12}$				
$\Delta_1$	$\Delta_2$	Estimate	CI length	Coverage	$\Delta_1$	$\Delta_2$	Estimate	CI length	Coverage
	0	1.0106	0.1729	0.9575		0	0.9966	0.216	0.925
0	0.75	1.0103	0.1738	0.9525	0	0.75	0.9993	0.2469	0.935
	1	1.0103	0.1742	0.9475		1	0.9957	0.2615	0.9525
	0	1.0125	0.1807	0.9525		0	0.9953	0.2395	0.9375
0.75	0.75	1.0123	0.1811	0.94	0.75	0.75	0.9975	0.2625	0.925
	1	1.0125	0.1814	0.95		1	0.9937	0.2775	0.955
	0	1.0139	0.1846	0.955		0	0.9943	0.2513	0.9425
1	0.75	1.0135	0.185	0.9475	1	0.75	0.9947	0.2739	0.9375
	1	1.0135	0.1854	0.9525		1	0.9912	0.2874	0.9475